JOURNAL OF GEOPHYSICAL RESEARCH
November 2005; 110(B11) : NIL_81-NIL_105
http://dx.doi.org/10.1029/2005JB003763

An edited version of this paper was published by AGU.

Crustal structure of the NE Rockall Trough from wide-angle seismic data modeling

F. Klingelhöfer[1], R. A. Edwards[1], R. W. Hobbs[1], R. W. England[2]

[1]Bullard Laboratories, University of Cambridge, Cambridge, UK
[2]Department of Geology, University of Leicester, Leicester, UK

Abstract: Two wide-angle seismic lines located in the northern Rockall Trough were acquired in May 2000. One line (line E) crosses the trough from the continental shelf off Lewis to normal oceanic crust west of Lousy Bank in NW-SE direction. The other line (line D) intersects with line E, crosses the Wyville-Thomson Ridge in a SW-NE direction and ends in the Faeroe-Shetland Basin. Sonobuoy data and expanding spread profiles acquired in the same area have been remodeled. Analysis of the seismic data using travel times and amplitudes reveals an up to 5 km thick sedimentary basin including an up to 1.5 km thick basaltic layer which is present in most of the trough. Further conclusions of this study are that the Rockall Trough is underlain by highly stretched continental crust of ~13 km thickness. The crust thickens to ~24 km beneath Lousy Bank, which is interpreted to be of continental nature. Beneath the Hebrides continental shelf a three-layer continental crust of 26 km is modeled. An up to 12 km thick high-velocity layer is observed underneath the ocean-continent boundary and is interpreted as magmatic underplating resulting from excess volcanism during rifting. No evidence for an underplate layer could be distinguished beneath the trough area. Modeling of the structure of the Wyville-Thomson Ridge revealed no existing igneous core of the ridge confirming existing theories, that it is a compressional structure.

Keywords: Rockall Trough; wide-angle seismics; crustal structure

1. Introduction

The Rockall Trough is a 250 km wide and up to 3 km deep bathymetric basin separating the Irish and UK continental shelves from the Rockall Bank (Figure 1). It is one of a series of rift basins that formed prior to the opening of the present day North Atlantic Ocean. To the north the Rockall Trough is separated from the Faeroe-Shetland Trough by the North-East Rockall Basin and the Wyville-Thomson Ridge. Early Tertiary continental break-up in the northern North-Atlantic was accompanied by massive extrusive volcanism due to the presence of the Iceland plume, as evidenced by a thick layer of flood basalts in the northern Rockall Trough *Barton and White* [1997]. In the last 10 years this region has been the focus of exploration for hydrocarbons which has required knowledge of the nature and thickness of the crust beneath the Trough and its rifting history. The new data presented here provides constraints on the nature and thickness of the crust and further knowledge of the development of aulacogens or failed attempts at rifting to form an ocean basins.

The age of the Rockall Trough has been subject to discussion. Ages derived from review of adjacent basins and plate reconstruction studies cover a wide range from the Torridonian *Roberts et al.* [1988], pre-Permian *Smythe* [1989], Late Carboniferous *Shannon et al.* [1995] to Cretaceous *Musgrove and Mitchener* [1996]; *England and Hobbs* [1997]. Evidence for pre-Cretaceous rifting in the Rockall Trough has been found from 2D structural and stratigraphic forward modelling *Nadin et al.* [1999]. The rift system might have continued into the Faeroe-Shetland Basin until the formation of the Wyville-Thomson Ridge through inversion in the mid-Tertiary *Boldreel and Andersen* [1993]; *Tate et al.* [1999].

The continental nature of the Rockall Plateau was first deducted from plate reconstructions *Bullard et al.* [1965]. This hypothesis has been subsequently verified by wide-angle seismic profiling *Scrutton* [1970]; *Bunch* [1979]. The crustal structure of deeper parts of the Rockall Trough has been derived mainly from wide-angle seismic data. In the absence of high quality deep crustal data, early work assumed oceanic crust in the middle of the trough (eg. *Talwani and Eldholm* [1977]). Analysis of two wide-angle seismic profiles crossing the Rockall Trough at 57^oN and 58.5^o N suggests that the deep basin is underlain by continental crust *Roberts et al.* [1988]. The two-layered continental crust is asymmetrically thinned in the centre of the Trough and the mid-crustal discontinuity is at its minimum depth closer to the thicker crust beneath the east margin and above the shallowest elevation of the Moho *Roberts et al.* [1988]. Data from two-ship seismic experiments in the centre of the Rockall Trough show a roughly 6 km thick crust *Joppen and White* [1990]. The authors conclude, also based on the interpretation of the two wide-angle profiles further to the north *Roberts et al.* [1988], that the crust in the area of the two-ship experiment is also of continental affinity. They do not exclude that part of the crust might be oceanic or might consist of intrusions from decompression melting *Joppen and White* [1990].

Using a seafloor cable recording explosive shots, the PUMA experiment confirmed that the three layered continental crust west of Lewis is about 26 km thick with either a sharp Moho discontinuity or a zone of high and low velocity laminations *Powell and Sinha* [1987]. Between 1987 and 1989 the United Kingdom Department of Trade and Industry acquired combined reflection, wide-angle and expanding spread seismic data from the UK mainland across the Hebrides Platform, Rockall Trough and Rockall Plateau. Analysis of

this data set revealed a velocity structure extending over the entire area of investigation which is consistent with continental crustal rocks, thinning from about 26 km underneath the UK mainland and Rockall Bank to 13.7 km in the Rockall Trough *Neish* [1993]. The crust is two-layered with a upper crustal layer of constant thickness across the Rockall Trough and pinching out at the ocean-continent boundary and a lower crust thickening underneath the shelf and underneath Rockall Bank *Neish* [1993].

Modelling of wide-angle and reflection seismic data in conjunction with expanding spread profiles revealed two series of seaward-dipping reflectors, consisting of submarine and subaerial lava flows and an up to 12 km thick high velocity layer underneath the Hatton Bank continental margin, interpreted as igneous underplating *Morgan and Barton* [1990]. The Rockall and Porcupine Irish deep seismic project carried out several deep reflection seismic and wide-angle surveys in the Hatton Basin and continental margin region. The main results of the modelling were the confirmation of the continental affinity of the crust in the Hatton Basin and the existence of a zone of thick lower crust below the Hatton margin east of anomaly 24, interpreted as underplated material *Vogt et al.* [1998]. Both the underplating and the seaward dipping reflectors can be explained by the volcanism caused by decompression melting of the passively upwelling asthenosphere underneath the thinning lithosphere during rifting. The main difference between volcanic and non-volcanic margins is the potential temperature of the asthenosphere, which is up to 150^o higher underneath volcanic margins *White et al.* [1987a]. Seismic methods have only detected underplating directly at the continent-ocean boundary, while subsidence analysis suggests regional underplating of 4-5 km thickness in the northern Rockall region *Brodie and White* [1994]; *Clift and Turner* [1998]. A layer consisting of velocities similar

to igneous underplating underneath the trough has been interpreted as a zone of extensive serpentinisation *O'Reilly et al.* [1996]. Subsequent remodelling of the data has not confirmed this interpretation *Pearse* [2002].

It has been inferred, that the Wyville-Thomson Ridge, Ymir Ridge and Bill Bailey's Bank are compressional ramp anticlines located above fault planes *Boldreel and Andersen* [1994]. This has been based on the observation that basaltic lavas with these structures are folded and that sedimentary sequences of the same age display onlap on one side of the structure and is uplifted and truncated on the other side. Ridge push from the initiation of sea-floor spreading in the North Atlantic has been proposed as cause for the NE-SW compressional stress necessary to form these structures *Boldreel and Andersen* [1994]. Recent investigations using reflection seismic data acquired in the region of the North East Rockall Basin show that the Wyville-Thomson Ridge has no igneous core and only a thin basalt cover overlying 3-4 km thick sedimentary layers *Tate et al.* [1999]. Based on these new data, the Wyville-Thomson Ridge together with the Ymir and Munkegrunnur ridges can be considered as positive inversion ramp-anticlines above an inferred mid-lower crustal detachment, generated during N-S intraplate compression *Tate et al.* [1999]. The origin of the deformation is proposed to be caused by compressional stress in the Pyrenean-Alpine foreland.

2. Seismic data

In May 2000 two wide-angle seismic lines were acquired by the Atlantic Margins Project (AMP) in the NE Rockall Trough (see Figure 2) using the R/V Akademic Boris Petrov and 50 ocean bottom seismographs (OBS) from Geopro GmbH. The main aims of the experiment were the study of the deep structure of the Rockall Trough and the ocean

continent transition zone as well as detection and quantification of magmatic underplate in the study area.

The main difficulty in imaging the deep structure of the crust in the Rockall Trough is the cover of basaltic lava flows, present across vast regions of the Trough. Since basalt is not deposited homogeneously scattering, reflection and attenuation of seismic energy are considerable. Furthermore, a basaltic layer often represents a high velocity layer, where the point of critical reflection is quickly reached preventing energy from penetrating the basalt layer. Sedimentary layers underneath the basalt then represent low velocity layers from which no energy is returned. The use of low frequencies and long offset data may help to overcome some of the difficulties. Therefore an experiment with ocean bottom seismometers was designed to record arrivals from a seismic source rich in low frequencies ensuring good penetration *Ziolkowski et al.* [2003].

A total of 66 successful deployments were undertaken on the two profiles. The instrument spacing on both profiles was on average 10 km. All instruments recorded on one vertical, two horizontal geophones and a hydrophone channel. The tuned airgun array, with the main frequencies centered around 8Hz, consisted of 10 air guns with a total volume of 3040 cu. in. (49.8 l), towed at a depth of 12 m. The shot interval was 60 seconds at an average speed of 4 knts., which translates to a trace spacing of about 120 m. The sample rate was 8 ms for all OBS. A total of 5576 shots (Line E: 3881, Line D: 1695) were fired by the airgun array.

Line E crosses the Rockall Trough from the continental shelf off Lewis extending over Lousy Bank and onto oceanic crust as defined by linear magnetic anomalies. It has a length of 480 km and 48 ocean bottom seismographs (OBS) from Geopro Gmbh were

used of which 45 yielded usable data. All shots on this profile were additionally recorded by British Geological Survey landstations, which allowed the profile to be extended to a length of 520 km using the data from landstation RTO which lies on the onshore projection of the profile.

Line D crosses Line E and ties with an existing BP/Shell data set which has been remodelled by the AMP. It was acquired using 20 OBS of which 19 yielded usable data and one was lost during the experiment. The line length is 180 km. The existing BP/Shell profile consists of 992 shots recorded by a total of 57 OBS, of which 45 provided useful data. The airgun array for the BP/Shell profile consisted of two airguns of 60 l each (a total of 7322 cu. in.). The same shot interval and sample rate were used as on Line D and E. The length of the combined D and BP/Shell profiles is 350 km.

Additionaly, the scope of the AMP experiment was enhanced by access to a previously unpublished dataset of combined expanding spread profile (ESP), sonobuoy and reflection seismic data acquired by the United Kingdom Department of Energy (DTi) in the Rockall Trough and Hatton Trough (Figure 2) which were reprocessed. The BANS 1 reflection profile crosses the continental margin of the Rockall Trough south of AMP Profile E at 59^o N onto oceanic crust. Four ESP profiles oriented at 90^o to the profile were used to constrain the deep velocity structure of the margin. A 7280 in^3 (120 litres) linear airgun array and a 4 km streamer with 300 channels were used during this survey. Four sonobuoys providing sufficiently long offsets (25km) of useful data, the seismic traces were redigitised from DTi paper sections to preserve amplitude information and included in the modelling.

3. Velocity modelling

Preprocessing of the data acquired for the Atlantic Margins Project undertaken by Geopro GmbH included calculation of the clock-drift corrections to adjust the clock in each instrument to the GPS base time. Instrument locations were corrected for drift from the deployment position during their descent to the seafloor by minimising the misfit between the predicted and recorded first water arrivals.

Data quality is very good on the western part of Line E overlying oceanic crust (Figure 3). Useful arrivals could be picked out to offsets of 120 km, including arrivals reflected from the top of a high velocity lower crustal layer and from the Moho. Due to the shallow water depth the data quality decreases over Lousy Bank, where multiples sometimes overlie secondary arrivals and strong reverberations can be observed in the vertical and horizontal channels of the OBS. In the Rockall Trough the data quality is variable, generally improving towards the eastern side of the trough where the basalt layer is thinner. The instruments located near to and over a hole in the basalt at 380 km model distance yield high quality data. Reflections from the Moho (PmP-arrivals) can be traced to offsets of 80 - 100 km (Figure 4). Landstation RTO (Figure 5) which has been included into the model recorded shots up to 150 km offset. Again due to very shallow water depth, the quality of the data on the continental shelf decreases towards the eastern end of the model.

The data quality along Line D is generally good (Figure 6) and improves towards the NE due to the thinning of the basaltic layer. Narrow bands of noise, possibly resulting from tidal currents are found on some sections. The quality of the BP/Shell data set is good throughout the line. The close spacing of the instruments allows a good correlation

of phases from one OBS to the next. Moho reflections or turning rays from the upper mantle were observed on 23 instruments along the line (Figure 7).

The data were modelled using the inversion and ray tracing algorithm of *Zelt and Smith* [1992]. Modelling was performed using a layer-stripping approach, proceeding from the top of the structure towards the bottom. We used a two-dimensional iterative damped least-squares inversion of travel times *Zelt and Smith* [1992]. Upper layers, where not directly constrained by arrivals from within the layer, were adjusted to improve the fit of lower layers. For the model parameterization we used the minimum-parameter/minimum structure approach to avoid inclusion of velocity or strucural features into the model unconstrained by the data *Zelt* [1999]. Lateral velocity changes are included into the model only if required by the data and layers are only included if reflected arrivals or changes in the velocity gradients are necessary to explain all arrivals. Velocity gradients and the phase identification in the velocity model were further constrained by synthetic seismogram modelling using asymptotic ray theory *Zelt and Ellis* [1988]. Picking of the onset of first and later arrivals was performed without filtering where possible (mostly between offsets of 0 - 40 km). Different filters were applied to the data where necessary, depending on the quality of the data and offset to the source.

Estimated picking uncertainties were 0.04 s for sedimentary and upper crustal turning ray arrivals, increasing to 0.06 s for mid- to lower crustal turning rays and reflected arrivals. The largest uncertainties were assigned to phases identified as resulting from diving rays into the upper mantle (P_n) or reflected on the Moho (P_m2P) or on the top of the igneous underplate (P_m1P). The number of picks, RMS traveltime residual and the χ^2 -error for all phases are listed in Table 1 for Line E and in Table 2 for Line D.

The final velocity model of Line E consists of 9 layers: the water layer, 2 sedimentary layers, one layer of basalt, three crustal layers, an underplate layer and the upper mantle layer. Each layer is defined by depth and velocity nodes. Water velocity is a constant 1500 m/s throughout the model, which agrees well with existing water velocity data *Dietrich et al.* [1975]. Seafloor bathymetry was determined from towed hydrophone data, due to the lack of digital echosounder logs. The seafloor model layer includes depth nodes at a spacing of 2.5 km (Figure 8). The two sedimentary layers found over oceanic crust and in the basin are modelled with the same node spacing. Sediment velocities range from 1900 m/s to 3800 m/s. In the trough a layer of basalt with a thickness up to 1.5 km has been modelled from the maximum distance of turning rays arriving from this layer and its amplitude with a velocity node spacing of 2.5 km overlying a third sedimentary layer with the same node-spacing. The velocity of the sub-basalt sediments could not be constrained, as this layer forms a low velocity zone and hence turning rays originating from this layer are not observed. The velocities of 3.00-3.80 km/s were assigned to this layer based on sediment velocities found where basalt was absent. The top of the basement has also been modelled with a node spacing of 2.5 km to account for its roughness. The mid-crustal layer, the top of the underplate layer and the Moho are less well resolved in the data and a depth node spacing of 10 - 12 km was adequate. Velocity nodes are only used when required by the model to account for lateral velocity variations, e.g. at the ocean-continent transition zone where normal oceanic crust with high velocity gradients changes to continental crust displaying much lower velocity gradients. A layer with velocities between 7.40 and 7.60 km/s, constrained by reflections from its top and bottom has been included in the model west of Lousy Bank and underneath the outer Hebrides shelf. Arrivals from diving rays

into the upper mantle were only observed on the landstation data and the upper mantle velocity is inferred to be constant throughout the model.

The final velocity model of Line D includes 10 layers, the water layer, two layers of sediments, a basaltic layer, an intermediate layer of sediments on top of a sill like layer, a fourth layer of older sediments, two crustal layers and the upper mantle layer (Figure 9). The water velocity is identical to that of Line E. The upper layer of sediments displays a velocity of 1.6 - 2.2 km/s, the second layer a velocity of 2.35 - 2.70 km/s. The boundary between the two layers is constrained by reflected arrivals from the boundary between them. Seafloor bathymetry from the towed hydrophone data and both sedimentary layers have been modelled using a node spacing of 2.50 km. The basaltic layer is generally thinner than on Line E, thinning eastward from around 700 m thickness to only 300 m thickness. The velocities are typical for basalt, around 4.20 - 4.80 km/s. The sediments underneath the basaltic layer have been modelled with velocities from 3.95 to 4.15 km/s and therefore represent a low velocity zone. Between model distance 130 km and 340 km a second high velocity layer with a subsequent velocity inversion to the underlying sedimentary layer has been modelled. The deepest sediments were modelled with a velocity of 4.20 to 4.70 km/s. Node spacing of the basaltic and lower sedimentary layers was 5 km. No reflections from the mid-crust interface have been found in the data so that no velocity discontinuity in the crust has been incorporated into the model. The crust consists of two layers, the upper crust displaying a velocity gradient from 6.0 - 6.4 km/s and the lower crust from 6.4 - 6.8 km/s. However a small discontinuity might have been undetected due to the data quality. Arrivals reflected from the Moho and from diving waves into the upper mantle have been identified throughout the dataset. The upper mantle velocity could thus be

constrained to 8.0 - 8.2 km/s. Node spacing at the Moho was around 20 km. At around 140 km model distance a deep reflection observed on four instruments has been included in the model as a mantle reflector.

4. Error analyses

Velocity gradients and the phase identification were constrained by synthetic seismogram modelling *Zelt and Ellis* [1988] (Figures 3, 4, 6, 7). In the synthetic seismograms the sedimentary layers typically generate low amplitude reflections, often overlain by multiple arrivals of the seabottom reflection. The layer of underplate underneath oceanic crust close to Lousy Bank gives a characteristic double reflection (Figure 3). The basaltic layer, where present, causes a high amplitude reflection and the high velocity gradient in this layer causes a high amplitude arrival out to offsets up to 20 km (Figure 6). The low velocity sediments underlying the basalt cause a characteristic stepback in the first arrival times, delaying the crustal turning rays (Figure 6). Since a low velocity layer does not produce turning rays, the constraints on this layer are generally weak. The high velocity gradients of the upper oceanic crust in the model give strong amplitude arrivals (Figure 3), while the lower gradients of the continental crust result in lower amplitude arrivals (Figure 4). The strong velocity contrasts across the Moho (P_mP) lead to a strong reflection visible on most data sections from Line E (Figure 4).

On Line D a late very high amplitude reflection can be observed, (Figure 6), which has been modelled as a mantle reflector. It is impossible to fit these arrivals as a Moho reflection and simultaneously construct a gravity model which satisfies the observed gravity data. The basaltic layer and the sill like body give rise to high amplitude arrivals (Figure 7).

Two-point ray-tracing between source and receiver (Figures 10 (a) and (b)) shows well resolved and unconstrained areas. On Line E the sedimentary layers and upper basement are well resolved throughout the model. Fewer reflected rays are seen from the mid-crustal and Moho discontinuity, the only major gap with no ray coverage of the Moho is between model distance 100 and 170 km and smaller gaps between 190 - 230 km and 340 - 370 km model distance. The depth of a mid-crustal velocity discontinuity is constrained by reflections between 0-80 km model distance and at distances greater than 300 km. Ray-coverage on Line D is good between model distance 80 and 350 km, however the Moho is not constrained by seismic data between 10 and 60 km model distance. No reflections from a mid-crustal discontinuity could be distinguished in the data, and the boundary represents a second order discontinuity with no associated velocity step in the model. For both lines the depth of the Moho has been additionally constrained by gravity modelling in those areas of insufficient ray coverage.

The fit between predicted arrival times and travel time picks provides information about the quality of the model (lower panels in Figure 10 (a), (b), (c) and Figure 11 (a), (b), (c)). The χ^2 is defined as the root-mean-square (rms) traveltime misfit between observed and calculated arrivals normalised to the picking uncertainty. The number of picks, picking error, the values for the χ^2 parameter and the rms misfit for the most important phases of the models are listed in Table 1 and Table 2.

Additional information about the quality of the velocity model can be gained from the resolution parameter (see Figure 12(a) and (b) *Zelt and Smith* [1992]. Resolution is a measure of the number of rays passing through a region of the model constrained by a particular velocity node and is therefore dependent on the node spacing. If a layer can

be modelled with one single velocity gradient the resolution parameter will be high even in areas which have lower ray coverage as the area is related to only one velocity node. The advantage of this representation is that it allows an assessment of whether all lateral velocity changes are required by the data. Hence, no structures unconstrained by the data have been included in the model *Zelt* [1999]. Nodes with values greater than 0.5 are considered well resolved (Figure 12(a)). The upper sedimentary layers and the upper crust of Line E are well resolved. Velocities of the low velocity layer underneath the basalt are not constrained by turning rays, thus this layer shows a low resolution. Although the lower crust is less well resolved than the upper crust, values are still well above 0.5 and can thus be considered reliable. Upper mantle velocities are only constrained by the landstation data and the resolution drops towards the western end of the profile. On Line D upper sedimentary, basaltic, upper crustal and upper mantle velocities have a resolution greater than 0.5 (Figure 12(b)). Again the low velocity zones underneath the basalt and the sills are unconstrained by turning rays and therefore show a lower resolution. The lack of turning rays in the lower crust leads to resolution values of 0.5 which can still be considered as sufficiently well resolved.

In order to estimate the velocity and depth uncertainty of the final velocity model a perturbation analysis was performed. The depths of key interfaces were varied and an F-test was applied to determine if a significant change between models could be detected. The 95% confidence limit gives an estimate of the depth uncertainty of the interface (Figure 12(a) and (b)). The top of the basaltic layer and the top of the basalt are very well constrained with an uncertainty of $\pm$ 60 m. The sill like body in Line D is less well

constrained with an uncertainty of ± 200 m due to the fact that it is located below a low velocity zone. Uncertainty of the Moho is around ± 0.5 km for both models.

To determine the robustness of our conclusions concerning the absence of the high velocity body underneath the trough, we constructed different velocity models including a model with a layer of underplate at 31.5 km depth, and a model with a layer of underplate of a constant thickness of 4 km and subsequently calculated synthetic seismograms for each model (Fig. 13). Both alternative models predict a double reflection from the top and base of the underplate with each a lower amplitude than the single high amplitude reflection predicted by the preferred velocity model, which is more consistent with the data observed.

In order to test whether a small region of oceanic crust is present in the middle of the trough, an alternative velocity model was produced. This model included higher, more oceanic type, velocity gradients in the middle of the trough. Comparison of synthetic seismograms from the final velocity model and the alternative velocity model indicates that the higher velocity gradients in the oceanic lower crust produce a stronger amplitude arrival then found in the data (Figure 14). We conclude from this that although arrival times found in the trough can be explained by oceanic crust as well as continental crust, the amplitudes of crustal arrivals are better explained by continental type crust. However, anomalous (highly intruded) or oceanic crust with an extent smaller than the OBS spacing cannot be excluded on the basis of the velocity modelling.

The different number of crustal layers between the two velocity models (Line E and Line D) at their intersection is a result of the minimum-parameter/minimum-structure modelling approach. We use only the smallest number of layers necessary to explain all

traveltime picks within their error bounds. As the velocity steps required to fully fit the data are relatively small on Line E (6.00 km/s to 6.20 km/s and 6.40 km/s to 6.60 km/s) it might not be possible to detect them on Line D. Small differences in top basement and Moho depths at the intersection of the lines are within the error bounds of the given interfaces (Figure 12).

5. Gravity modelling

Assuming seismic velocities and densities can be correlated, gravity modelling provides important additional constraints on the seismic model. Areas unconstrained by the seismic data can be modelled by comparing calculated gravity anomalies with those observed. Crustal P-wave velocities from the seismic models were converted to densities using the relationship of Christensen and Mooney (1995) with upper mantle densities set to a constant 3.32 g/cm^3. Sedimentary velocities were converted to densities using the different empirical relationships for sedimentary layers *Hamilton* [1978]; *Hughes et al.* [1998]; *Ludwig et al.* [1970] (Figure 15). Gravity anomalies along the profiles were extracted from the satellite derived gravity dataset of *Sandwell and Smith* [1995] (Figure 16). The gravity data were forward modelled using the 2.5D GRAVMAG gravity and magnetic modelling software developed by the British Geological Survey *Pedley et al.* [1993]. To avoid edge effects both models have been extended by 100 km at both ends and down to a depth of 95 km.

The Line E gravity model consists of 17 polygons. Densities used for the modelling are shown in Figure 15. The background density has been set to 2.94 g/cm^3, the average density of the model. The upper crust of the gravity model has a density of 2.80 g/cm^3, densities on top of Lousy Bank are slightly less, corresponding to the lower seismic ve-

locities. The density of the lower crust in the oceanic part of the model is 3.05 g/cm^3. Lower densities have been assigned to the lower crust in the centre of the trough. Underneath the Outer Hebrides Shelf the model requires higher densities. This is reflected in the higher crustal velocities in this region. The base of the crust displays velocities up to 7.2 km/s which translate into densities of 3.05 kg/m^3 *Christensen and Mooney* [1995]. A possible explanation for this slightly elevated velocity and density might be an intrusion in the lower crust or a layer of magmatic underplate, which grades into the lower crust rather than having a sharp boundary, as only few reflections from the top of the possible underplate layer are found in the seismic data in this region, in contrast to the NW end of the line. Here the best fit to the observed gravity can be obtained by assigning a density of 3.1 g/cm^3 to the high velocity layer found under the oceanic part of the data and Lousy Bank itself. No indications are found from either the seismic or the gravity modelling for a thick layer of underplate beneath the centre of the trough. The fit between the gravity anomaly predicted from the modelling and the free air gravity anomaly calculated from satellite altimetry is generally good. The largest discrepancy is found between model distance 120 and 180 km and is probably due to a gravity high slightly south of the profile (Figure 16).

Densities on Line D are similar to those on Line E (Figure 18). Sedimentary densities were chosen between 2.20 and 2.40 g/cm^3, the basaltic layer and the sill density as 2.50 g/cm^3. The upper crustal layer with a density of 2.70 g/cm^3 is a mean density between the two upper crustal layers of Line E. The lower crust has a density of 2.90 g/cm^3 similar to the lower crust on Line A and E. The upper mantle has been set to 3.32 g/cm^3. The overall fit is good and there was no need to divide the seismic layers into different density

layers. Both ends of the model show an increasing misfit. At the NE end this is due to the influence of the Westray ridge. At the SW end the misfit is probably due to increasing basement depth.

6. Reprocessing of the BANS dataset

The ESP and sonobuoy data were forward modelled using the same software as for Line E and Line D *Zelt and Smith* [1992]. In order to be able to interpolate between the sonobuoys and ESPs the main reflectors were digitised from the confidential coincident deep seismic reflection sections, including up to three sedimentary layers, a basaltic layer, basement and in some Moho reflections. The travel-times were converted to depth using the seismic velocities from the sonobuoy and ESP data and the reflectors were subsequently incorporated into the wide-angle seismic modelling (Figure 19a).

The fact that sonobuoys are subject to drift with the prevailing ocean currents after deployment can introduce significant travel-time errors into the modelling. The true offset between the sonobuoy and the ship can be calculated using the direct arrival traveling through the water column with the precisely known water-velocity. It is then possible to recalculate the offsets for the complete section. One assumption made was that drift was linear at a constant speed throughout the active life span of the instrument. Using this simple correction it was possible to reduce the average travel time error for the direct water wave and the reflections from the seafloor from 150 ms to 80 ms, on all profiles. The signal/noise-ratio in the sonobuoy section is generally lower than in an OBS section due to the wave generated noise being sourced closer to the instruments and the fact that the sound waves have to cross the water column twice. Data quality on the instruments

used for the modelling is generally good for the sonobuoy data, however, on the BANS profile no deep crustal arrivals could be picked.

For the expanding spread profiles, the shooting and receiving vessels start from a common mid-point and travel apart maintaining equivalent shot and receiver distances along the track. As the distance between the ships increases the first arrival soundwave originates from greater depths. Explosives were used as the source with an increased charge from 10 kg to 400 kg along each 92 km long profile. Usually expanding spread profiles are modelled as one dimensional velocity depth profiles, assuming structure is 1-D underneath the midpoint of the profile. Accordingly, the profiles should be shot parallel to any bathymetric or structural feature, rather than across it, in order to find true seismic velocities. While BANS ESPs 02, 05 06 and V88-6 were shot parallel to the margin, ESP 04 was shot across the margin, where clearly the assumption of 1-dimensionality is not valid.

In order to be able to allow for varying bathymetry on the ESP 04 for which the 1-dimensionality assumption is not valid and to include 2-D crustal structure, the shots of each ship were binned into 9 average shotpoints with 10 km distance between them, gradually increasing from the starting shot point. Real shot-receiver offsets were used for the modelling, with the bin shifting along with the shooting vessel, in order to keep the deepest penetrated point underneath the midpoint of the profile. This method allows varying subsurface structure to be taken into account. ESP 02, 05, 06 and 88 for which the 1 dimensionality assumption is likely to be valid, were modelled one dimensionally using the same software and the final velocity depth profiles were subsequently incorporated into the main profile at the intersection points.

Data quality for all of the ESP is very good with clear arrivals up to the maximum shot offset of 70 km. ESP 06 and 02 display a clear double reflection around 6s reduced travel-time (Figure 20). Where previously seen this has been interpreted as indicative of the presence of underplate *White et al.* [1987b]. Unfortunately a mute has been applied to the BANS ESPs, which has erased the first arrivals at offsets between 20 and 30 km, so that the shallow crustal velocities are mainly constrained by the sonobuoy data.

Because of the lower signal/noise-ratio of the sonobuoys compared to OBSs or ESPs and to allow for travel-time errors due to drift remaining in the data after correction, the picking error for the sonobuoy data was set at 80 ms for all phases, which is slightly higher than for the ocean bottom instruments. The same picking error was used for the ESPs. For the longer offsets the 80 ms error is comparable to that of ocean bottom seismometers. The increase in noise due to the double crossing of the water column is compensated by the stacking of the streamer traces. The number of picks, RMS traveltime residual and the χ^2 -error for all phases are listed in Table 3 for the BANS 1 and the 1D ESP Profiles.

Because of the greater instrument spacing and poorer data quality of the sonobuoys, only five layers have been distinguished and are shown in the final velocity models for the BANS profile (Figure 19b). These include one sedimentary layer (2 - 2.5 km/s), a basaltic layer with velocities from 4.5 to 5.5 km/s, and two crustal layers (5.60 - 6.00 km/s and between 6.00 and 6.40 km/s to 6.60 km/s), a high velocity body (7.00 to 7.40 km/s), and an upper mantle layer (Figure 19b). The high velocity body has been modelled from a double reflection, seen in ESP 02 and ESP 06 data sections (Figure 20). Interpolation between the two ESPs was achieved using gravity modelling. No indications of this body could be detected in ESPs 04, 05, and V88-6, although all of them show a clear reflection

from the Moho. Therefore, this body was not included in the model from the ESP data. Upper mantle velocities were not constrained by the seismic data and were set to 8.00 km/s.

Although the model is less well-constrained than the Line E and D velocity models and raycoverage is sparse in some regions (Figure 19c), the existence of a high velocity body underneath the ocean-continent transition zone is well-constrained by the double reflection seen in two ESP. To futher resolve the crustal structure and the thickness of the underplate in areas unconstrained by wide-angle seismic data, gravity modelling has been performed using the approach described for Line E and Line D. The resulting fit between the predicted anomaly and the observed satellite gravity data is good (Figure 19e), resulting from the fact that the seismic constraints were less tight leaving more space for changes to fit the gravity anomaly. The slight residual misfits could be due to 3D or edge effects.

7. Results and discussion

At the western end of Line E two sedimentary layers of 1.5 km thickness overlie a layer with velocities typical of basaltic rocks (Figure 21). On Lousy Bank, where this layer crops out analog echo sounder recordings show a rough seafloor typical of basaltic lava flows, which can be correlated with the top of the basalts to the west. Beneath the sediments, a two layer igneous crust is imaged, with velocity gradients and relative thicknesses characteristic of oceanic crust. However its total thickness of ca. 15 km is unusually thick for oceanic crust *White et al.* [1992]. This might be explained by thick crust formed at the beginning of sea floor spreading in the presence of a mantle plume *White and McKenzie* [1989]. Oceanic crust along the Hatton margin to the SW exhibits a

comparable thickness of 11 km *Morgan and Barton* [1990]. Underneath the oceanic crust, an 8 km thick layer displaying velocities higher than normal crustal velocities but lower than normal mantle velocities has been imaged. This layer is interpreted to be igneous underplating from the initial rifting. Bodies of similar size and seismic velocity have been described below the Hatton Bank margin *Morgan and Barton* [1990]. These velocities correspond neither to mantle material nor to normal oceanic gabbro which has velocities of 6.8–7.2 km/s. Underplated gabbros derived from melting of asthenosphere with unusually high potential temperature can have increased velocities *White and McKenzie* [1989]. Alternatively, the high-velocity material might correspond to gabbro sills alternating with dunites *Canales et al.* [2000] or to olivine-rich gabbros resulting from fractionation of basaltic melt *Farnetani et al.* [1996].

The character of the crust changes towards Lousy Bank, where the velocity gradients are shallower and the crust is divided into two layers of roughly similar thickness with velocities between 6.2-6.4 km/s at the Hebrides shelf end of the profile and 5.75-6.40 km/s at Lousy bank for the upper crustal layer and 6.6-6.8 km at both ends of the line for the lower crustal layer. These velocities are more characteristic of continental crust than of a volcanic edifice. The lower velocities near the top of the crust at Lousy Bank can be explained by lower burial pressures allowing joints to remain open. In addition to the similar velocities found beneath the Outer Hebrides Shelf and Lousy Bank the maximum crustal thickness at Lousy Bank is 26 km, only slightly thinner than underneath the Shelf. From this it is concluded, that the crust at Lousy Bank is of continental origin, which is also in good agreement with previous work which found Rockall Bank south of Lousy Bank to be continental in nature *Roberts et al.* [1988]. In contrast,

oceanic plateaus usually display units having velocities typical of oceanic layers 2 and 3 with velocities corresponding to layer 3 occurring at shallower depth than in continental fragments *Carlson et al.* [1980].

In the centre of the trough, the sedimentary layers thicken from 2 to 5 km. A thick layer of basalt (up to 1.5 km) can be found in the trough at depths of 2-4 km. The basalt is underlain by a sediment layer up to 2 km thick. The crust thins asymmetrically to around 12 km thickness towards the centre of the trough, with shallowest Moho close to the continental Outer Hebrides Shelf area to the East. The nature of the crust itself does not change, displaying gradients typical for continental crust throughout the Trough. The mid-crustal reflection reaches its shallowest point at the same location, indicating probably that stretching was highest in this area. A very similar asymmetric crustal geometry has been found in the Rockall Trough slightly further to the south *Roberts et al.* [1988]. The crustal thickness increases to 32 km at the eastern end of the profile underneath the continental shelf area. Here it displays three layers with a velocity of 6.0-6.2, 6.2-6.4, and 6.6-7.2 km/s respectively. The thickness and partitioning is comparable with that previously found west of the Outer Hebrides *Powell and Sinha* [1987] and is believed to be typical of Lewisian basement. The slightly elevated velocity at the base of the crust could be explained by magmatic intrusion into the crust during rifting. A second region of underplating has been modelled underneath the continental shelf, mainly constrained by a double reflection seen on the data recorded by the landstation RTO (Figure 5).

The thickness of the sedimentary layer in the BANS profile varies from a few hundreds of meters in the east to two kilometers in the western part of the profile (Figure 21). Underneath the sedimentary layer, a basalic layer has been modelled, which thins towards

the west from 3 km thickness and ends at 100 km model distance. A seaward dipping reflection (SDR) sequence, resulting from basaltic lava flows being erupted on the subsiding continental margin during initial opening of the ocean are imaged in the coincident reflection seismic data at 100 km model distance (19). The velocity model shows a 18 km thick continental crust at the eastern end of the profile (Figure 21). This crust thins gradually to about 5 km thickness underneath a thick sequence of SDRs at about 100 km model distance. The crust westward of these SDRs is interpreted to be of oceanic origin. The velocity gradient in the lower crustal layer increases oceanwards, typical for the transition to oceanic crust, although the lower crustal velocities might be slightly lower than for typical oceanic crust. This is in good agreement with the normal oceanic crustal thickness of 7 km found in this region. Between 30 km and 180 km model distance the crust is underlain by an up to 10 km thick high-velocity body interpreted to be magmatic underplating similar to the underplate body found on Line E.

Sedimentary layers on Line D display a thickness of 5.5 km at the SW end of the profile and thicken in the NE Rockall basin to 8 km thickness at 145 km model distance (Figure 21). The thickness decreases towards the NE to about 5 km at 300 km model distance. The thickness of the basaltic layer is less than on Line E and it thins towards the northeast. A second high velocity layer in the sediments may consist of several sill complexes which cannot be resolved individually. Where the profile crosses the Wyville Thompson Ridge both high velocity layers are parallel folded, confirming a compressional origin for the Ridge. Additionally, small basement highs are located underneath the Wyville-Thompson and the Ymir ridges, and no large igneous core (high velocities) is needed to model the ridges, casting doubt on an igneous origin for the Ridges themselves. The crustal thickness

along Line D increases from 10 km to 14 km towards the NE. The velocities and velocity gradients in the crust throughout the model are characteristic of continental type crust. No indications of a high velocity body which could be interpreted as igneous underplating have been found in the model of Line D and diving rays into the mantle show, where present, a normal mantle velocity of 8 km/s. A deep high amplitude reflection is observed between 120 and 160 km model offset. It corresponds in depth to a deep reflection found in the southern Rockall Trough interpreted to be the boundary between serpentinised and normal upper mantle material. However, mantle velocities above the reflector are around 8 km/s on Line D. This excludes igneous underplating as well as serpentinisation of the upper mantle as possible explanations for the origin of this reflector. This reflector is not imaged on Line E, which excludes its lateral continuity between both lines. Because no velocity contrast across this boundary could be observed it is interpreted as an mantle reflection rather than the base of an underplate layer.

8. Comparison to published datasets

The PUMA experiment *Powell and Sinha* [1987] was located off the coast of northern Britain to the west of the Outer Hebrides (Figure 2) over high velocity, seismically homogeneous, non-reflective, Lewisian basement. A new type of sea-bottom receiver, the PUMA, consisting of an 1100 m long array of hydrophones deployed at the seabed was used as the main receiver. The endpoint of the PUMA profile is located about 40 km SW of Line E OBS 47. The modelled 1-D velocity-depth relationship from the PUMA data agrees well with the velocity-depth function at the western end of Line E (Figure 22). The difference in depth of the mid-crustal and Moho reflectors is about 1 km and that of the Moho depth is even smaller. No evidence of underplate was detected in the PUMA data

and an upper mantle velocity of 8 km/s has been modelled using data collected during the PUMA experiment from two landstations on Lewis.

Roberts et al. 1988 present models for two wide-angle seismic profiles across the northern Rockall Trough (Figure 2). The main aims of the project were the determination of the crustal structure and the characterisation of the nature of the crust beneath the trough. Profile P2 crosses the Rockall Trough south of Line E and the observed crustal structures are similar on both lines (Figure 23). On Line P2 an eastward dip of the sediment covered basement and a thinning of the crust on the western flank of the trough is observed, comparable to the thinning of the crust west of Lousy Bank on Line E. A general asymmetry of the trough with the shallowest Moho adjacent to the eastern margin of the trough, dipping gently to the west can be found in both models. Crustal thicknesses along both profiles are nearly identical; starting on the western flank with a crustal thickness of about 22 km, thinning in the trough to 11 km and then thickening to around 30 km (Figure 23). No underplating has been detected along profile P2, although areas where underplating could be expected beneath the thicker crust at the margins of the trough are generally unconstrained by the seismic data. Both models show a two-layered crust displaying velocity gradients typical for thinned continental crust and the depth of the mid-crustal reflector is comparable in both lines.

Drill holes can provide a correlation between seismic velocities and the lithology of the observed layers (Figure 2). The BP Drill hole 154/3-1 is located 70 m from OBS 43 on Line E. Drilling penetrated a basaltic layer and ended in Lewisian gneiss. Both the depth of the basaltic layer and depth of the top Lewisian Gneiss agree well with the velocity model

at OBS 43 (Figure 24). A 400 m thick layer of sediments, representing a low-velocity layer underneath the basalt, could not be resolved in the seismic model.

9. Conclusions

Modelling of the wide-angle data along two profiles in the northern Rockall Trough reveals a two-layered thinned continental crust underlying the trough. Velocity gradients between 5.6 - 6.4 km/s and 6.6 - 6.8 km/s confirm this. The crustal thickness inceases underneath Lousy Bank to about 26 km, only 4 - 5 km less than undeformed continental crust in this region. From the velocity gradients this is interpreted to be of continental origin rather than oceanic origin and is consistent with knowledge of the nature of the adjacent Rockall Bank *Bullard et al.* [1965]; *Bunch* [1979]. Thin crust with velocity gradients characteristic of oceanic crust have been found west of Lousy Bank suggesting that the ocean-continent boundary lies to the west.

Underneath the ocean-continent boundary a body with velocities between 7.4 - 7.6 km/s has been imaged on Profile E and the Bans ESP data. It is constrained in both datasets by a characteristic double reflection from its top and base. This body is interpreted to consist of magmatic underplate, produced by excess mantle melting that accompanied the opening of the NE Atlantic ocean. Similar bodies have been found further south on this margin *White et al.* [1987a]; *Barton and White* [1997]. However, no evidence for magmatic underplating beneath the NE Rockall Trough has been found in this study, contrary to interpretations based on subsidence analysis *Brodie and White* [1994]; *Clift and Turner* [1990]. Equally, no evidence for a high degree of serpentinisation in the mantle underneath the Rockall Trough has been found as proposed to exist in the southern Rockall Trough *O'Reilly et al.* [1996].

Finally, modelling of the structure of the Wyville Thomson Ridge revealed no existing igneous core of the ridge confirming interpretations of gravity and reflection seismic data *Tate et al.* [1999]; *Waddams and Cordingley* [1999], that this is a compressional structure.

Acknowledgments. We thank the captain and the crew of the R/V Boris Petrov. Acquisition and processing of the data was funded by the Atlantic Margins Project's Industrial Sponsors: Amerada Hess Ltd, BP Exploration Operating Co. Ltd, Conoco (UK) Ltd, TotalFinaElf UK, Lasmo North Sea plc, ExxonMobil North Sea plc, Shell UK Exploration and Production, Statoil UK Ltd. The GMT software package *Wessel and Smith* [1995] was used in the preparation of this paper.

References

Barton, A. J., and R. S. White, Crustal structure of Edoras Bank continental margin and mantle thermal anomalies beneath the North Atlantic, *J. Geophys. Res., 102*, pp. 3109–3129, 1997.

Boldreel, L. O., and M. S. Andersen, Late Paleocene to Miocene compression in the Faeroe-Rockall area, *Petroleum Geology of Northwest Europe: Proceedings of the 4th Conference*, pp. 1025–1034, 1993.

Boldreel, L. O., and M. S. Andersen, Tertiary development of the Faeroe-Rockall Plateau based on reflection seismic data, *Bull. Geol. Soc. Denmark*, pp. 162–180, 1994.

Brodie, J., and N. White, Sedimentary basin inversion caused by igneous underplating on the Northwest European continental shelf, *Geology, 22*, pp. 147–150, 1994.

Bullard, E. C., J. E. Everett, and A. G. Smith, The fit of the continents around the Atlantic, *Philos. trans. R. Soc. London, Ser. A, 258*, pp. 41–52, 1965.

Bunch, A. W. H., A detailed seismic structure of Rockall Bank (55^on, 15^ow) - A synthetic seismogram analysis, *Earth Planet. Sci. Lett., 45*, pp. 453–463, 1979.

Canales, J. P., R. S. Detrick, J. Lin, and J. A. Collins, Crustal and upper mantle seismic structure beneath the rift mountains and across a nontransform offset at the mid-atlantic ride (35^o n), *J. Geophys. Res. 105*, pp. 2699–2719, 2000.

Carlson, R. L., and C. N. Herrick, Densities and porosities in the oceanic crust and their variations with depth and age., *J. Geophys. Res. B, 95*, pp. 9153–9170, 1990.

Carlson, R. L., N. I. Christensen, and R. P. Moore, Anomalous crustal structures in ocean basins: Continental fragments and oceanic plateaus., *Earth Planet. Sci. Lett., 51*, pp. 171–180, 1980.

Christensen, N. I., and W. D. Mooney, Seismic velocity structure and composition of the continental crust; a global view, *J. Geophys. Res., 100, 6*, pp. 9761–9788, 1995.

Clift, P. D., and J. Turner, The thermal impact of Paleocene magmatic underplating in the Faroe-Shetland-Rockall region, *Petroleum Geology of Northwest Europe: Proceedings of the 5th Conference*, pp. 585–593, 1990.

Clift, P. D., and J. Turner, Paleogene igneous underplating and subsidence anomalies in the Rockall-Faeroe-Shetland area, *Mar. Pet. Geol.*, pp. 223–243, 1998.

Dietrich, G., K. Kalle, W. Krauss, and G. Siedler, Allgemeine Meereskunde, *Bortraeger, Berlin*, pp. 259–264, 1975.

England, R. W., and R. W. Hobbs, The structure of the Rockall Trough imaged by deep seismic reflection profiling, *J. Geol. Soc. Lond., 154(3)*, pp. 497–502, 1997.

Farnetani, C. G., M. A. Richards, and M. S. Ghiorso, Petrological models of magma evolution and deep crustal structure beneath hotspots and flood basalt provinces, *Earth*

Planet. Sci. Lett. 143, pp. 81–94, 1996.

Hamilton, E. L., Sound velocity-density relations in the sea-floor sediments and rocks, *J. Ac. Soc. Am., 63*, pp. 366–377, 1978.

Hughes, S., P. J. Barton, and D. Harrison, Exploration in the Shetland-Faeroe Basin using densely spaced arrays of ocean-bottom seismometer, *Geophys., 63, 2*, pp. 328–334, 1998.

Joppen, M., and R. S. White, The structure and subsidence of Rockall Trough from two-ship seismic experiments, *J. Geophys. Res., 95 (B12)*, pp. 19,821–19,837, 1990.

Ludwig, J. W., J. E. Nafe, and C. L. Drake, Seismic refraction, *The Sea, 4, 1*, pp. 53–84, 1970.

Morgan, J. V., and P. J. Barton, A geophysical study of the Hatton Bank volcanic margin: a summary of the results from a combined seismic, gravity and magnetic experiment, *Tectonophysics, 173*, pp. 517–526, 1990.

Musgrove, F. W., and B. Mitchener, Analysis of the pre-Tertiary rifting history of the Rockall Trough, *Petroleum Geoscience, 2*, pp. 353–360, 1996.

Nadin, P. A., M. A. Houchen, and N. J. Kusznir, Evidence for pre-Cretaceous rifting in the Rockall Trough: an analysis using quantitative 2d structural/stratigraphic modelling, *Petroleum Geology of Northwest Europe: Proceedings of the 5th Conference*, pp. 371–378, 1999.

Neish, J. K., Seismic structure of the Hatton-Rockall area: an integrated seismic/modelling study from composite datasets, *Petroleum Geology of Northwest Europe: Proceedings of the 4th Conference*, pp. 1047–1056, 1993.

O'Reilly, B. M., F. Hauser, A. W. B. Jacob, , and P. M. Shannon, The lithosphere below the rockall trough: wide-angle seismic evidence for extensive serpentinisation,

Tectonophys., 255, pp. 1–23, 1996.

Pearse, S., Inversion and modelling of seismic data to assess the evolution of the Rockall Trough, *Ph. D. Thesis, Univ. of Cambridge*, p. 225, 2002.

Pedley, R. C., J. P. Busby, and Z. K. Dabek, GRAVMAG User Manual - interactive 2.5d gravity and magnetic modelling, *British Geological survey, Technical Report WK/93/26/R*, pp. 497–502, 1993.

Powell, C. M. R., and M. C. Sinha, The PUMA experiment west of Lewis, UK, *Geophys. J. R. astr. Soc., 89*, pp. 259–264, 1987.

Roberts, D. G., A. Ginzberg, K. Nunn, and R. McQuillin, The structure of the Rockall Trough from seismic refraction and wide-angle measurements, *Nature, 332*, pp. 632–635, 1988.

Sandwell, D., and W. Smith, Marine gravity from satellite altimetry, *The Geological Data Center, Scripps Institution of Oceanography, La Jolla, CA92093 (digital file, version 7.2), (anonymous ftp to baltica.ucsd.edu)*, 1995.

Scrutton, R. A., Results of a seismic refraction experiment on Rockall Bank, *Nature, 227*, pp. 826–827, 1970.

Shannon, P. M., A. W. Jacob, J. Makris, B. O'Reilly, F. Hauser, and U. Vogt, Basin development and petroleum prospectivity of the Rockall and Hatton region, *The petroleum Geology of Irelands offshore basins. Geol. Soc. London Spec. Publ., 93*, pp. 435–457, 1995.

Smith, W., and D. Sandwell, Global seafloor topography from satellite altimetry and ship depth soundings, *Science 277*, pp. 1956–1962, 1997.

Smythe, D. K., Rockall Trough - Cretaceous or Late Paleozoic?, *Scottish J. Geol., 25*, pp. 5–43, 1989.

Stoker, M., K. Hitchen, and C. C. Graham, The geology of the Hebrides and West Shetland shelves, and adjacent deep-water areas., *BGS, UK Offshore Regional Rep., HMSO, London*, 1993.

Talwani, M., and O. Eldholm, Evolution of the Norwegian-Greenland Sea, *Geol. Soc. Am. Bull.*, pp. 969–999, 1977.

Tate, M. P., C. D. Dodd, and N. T. Grant, The northeast Rockall Basin and its significance in the evolution of the Rockall-Faroes/East Greenland rift system, *Petroleum Geology of Northwest Europe: Proceedings of the 5th Conference*, pp. 391–406, 1999.

Vogt, U., J. Makris, B. M. O'Reilly, F. Hauser, P. W. Readman, and A. W. B. Jacob, The Hatton Basin and continental margin: Crustal structure from wide-angle seismic and gravity data, *J. Geophys. Res., 103(B6)*, pp. 12,545–12,556, 1998.

Waddams, P., and T. Cordingley, The regional geology and exploration potential of the NE Rockall Basin, *Petroleum Geology of Northwest Europe: Proceedings of the 5th Conference*, pp. 379–390, 1999.

Wessel, P., and W. H. F. Smith, A new version of the Generic Mapping Tool (GMT), *EOS, Trans. Am. Geophys. Un., 76*, p. 329, 1995.

White, R. S., and D. McKenzie, Magmatism at rift zones: The generation of volcanic continental margins and flood basalts, *J. Geophys. Res., 94(B6)*, pp. 7685–7729, 1989.

White, R. S., G. D. Spence, S. R. Fowler, D. P. McKenzie, G. K. Westbrook, and A. N. Bowen, Magmatism at rifted continental margins, *Nature*, pp. 439–444, 1987a.

White, R. S., G. H. Westbrook, A. N. Bowen, S. R. Fowler, G. D. Spence, C. Prescott, P. J. Barton, M. Joppin, J. Morgan, and M. H. P. Bott, Hatton bank (northwest U.K.) continental margin structure, *Geophys. J. R. Astron. Soc., 89*, pp. 265–272, 1987b.

White, R. S., D. McKenzie, and R. O'Nions, Oceanic crustal thickness from seismic measurements and rare earth element inversions, *J. Geophys. Res. 97*, pp. 19,683–19,715, 1992.

Zelt, C. A., Modelling strategies and model assessment for wide-angle seismic traveltime data, *Geophys. J. Int. 139*, pp. 183–204, 1999.

Zelt, C. A., and R. M. Ellis, Practical and efficient ray tracing in two-dimensional media for rapid travel time and amplitude forward modelling, *Can. J. Explor. Geophys. 24*, pp. 16–34, 1988.

Zelt, C. A., and R. B. Smith, Seismic travel time inversion for 2-d crustal velocity structure, *Geophys. J. Int. 108*, pp. 16–31, 1992.

Ziolkowski, A., P. Hanssen, R. Gatliff, H. Jakubowicz, A. Dobson, G. Hampson, L. Xiang-Yang, and L. Enru, Use of low frequencies for sub-basalt imaging, *Geophysical Prospecting, 51*, pp. 169–182, 2003.

10. Figure Captions

Figure 1: Continental margin west of Britain. Bold line show wide-angle profiles and major physiographic features are shown. Contours (250 m contour interval) are predicted seafloor bathymetry from satellite gravity *Smith and Sandwell* [1997].

Figure 2: Location map of the Line E and D and the BP/Shell-data set. Inverted triangles show location of OBS recovered successfully on Line E and D. Circles show successful recovery locations of OBS from the BP/Shell line used to extend Line D. Black dashed

line marks the eastward extend of the basalt and the hole in the basalt (after *Stoker et al.* [1993]). Black triangle shows BGS landstation location. Circles mark sonobuoy position on the BANS-1 Profiles and stars the midpoints of the ESP used for the modelling. Position of the BP drill hole 154/3-1 is marked by a diamond. Contours are predicted seafloor bathymetry from satellite gravity *Smith and Sandwell* [1997] in an 250m intervall.

Figure 3: (a) Bandpass filtered (3-5 Hz, 24-36 HZ) data from the hydrophone channel of OBS 01 (Hydrophone) on Line E. The data are gain-adjusted according to offset and reduced to a velocity of 6 km/s. (b) Synthetic seismograms calculated from the final velocity model for the same OBS using asymptotic ray theory code *Zelt and Smith* [1992]. The synthetic seismograms are spaced at a 500 m interval and the same offset-dependent gain has been applied as to the seismic data. The wavelet consists of a 29-point low-passed Ricker wavelet. P-wave quality factors were chosen to be 100-200 for sedimentary layers, 400 for the basaltic layers and upper crust, 700 for the lower crust and 1000 for the upper mantle.

Figure 4: (a) Data from the hydrophone channel of OBS 38 for Line E with same gain, filter and scaling applied as in Figure 3 (b) the corresponding synthetic seismograms.

Figure 5: (a) Data from vertical geophone channel of the landstation RTO. The data are gain-adjusted according to offset and reduced to a velocity of 8 km/s.

Figure 6: (a) Data from the hydrophone channel of OBS 06 for Line D with same gain, filter and scaling applied as in Figure 3 (b) the corresponding synthetic seismograms.

Figure 7: (a) Data from the hydrophone channel of OBS 42 from the BP/Shell data set with same gain, filter and scaling applied as in Figure 3 (b) the corresponding synthetic seismograms.

Figure 8: Final velocity model of Line E including the model boundaries used during inversion (solid lines) and isovelocity contours every 0.25 km/s. Positions of OBSs (inverted triangles) are indicated.

Figure 9: Final velocity model of Line D and BP/Shell datasets including the model boundaries used during inversion (solid lines) and isovelocity contours every 0.25 km/s. Positions of OBSs (inverted triangles) are indicated.

Figure 10: (a) Upper panel: Ray coverage of the model of Line E for the sedimentary layers, with every 20^{th} ray from point-to-point raytracing. Positions of the receivers are indicated by inverted triangles. Lower panel: fit between the travel time picks (dark grey bars) and the predicted arrival times (black lines) from raytracing for the sedimentary layers (b) As above for the upper crustal layer (c) As above for the lower crustal and upper mantle layers.

Figure 11: (a) Upper panel: Ray coverage of the model of Line D BP/Shell for the sedimentary layers, with every 20^{th} ray from point-to-point raytracing. Positions of the receivers are indicated by inverted triangles. Lower panel: fit between the travel time picks (dark grey bars) and the predicted arrival times (black lines) from raytracing for the sedimentary layers (b) As above for the upper crustal layer (c) As above for the lower crustal and upper mantle layers.

Figure 12: (a) Resolution parameter for all depth nodes of the velocity model of Line E. Velocity nodes are marked by green circles and OBS positions by stars. Contour interval is 0.1. Depth uncertainty of the most important model boundaries as determined by 95% confidence of the F-test during depth perturbation of the boundary. The depth uncertainty of the most important boundaries calculated from the 95 % confidence limit of

the f-test given in the framed boxes. (b) Resolution parameter for all depth nodes of the velocity model of Line D. Velocity nodes are marked by green circles and OBS positions by inverted triangles. Contour interval is 0.1. The depth uncertainty of the most important boundaries calculated from the 95 % confidence limit of the f-test is given in the framed boxes.

Figure 13: (a) Vertical geophone section of OBS 38. (b) Synthetic seismograms calculated from the final velocity model shown in inset. (c) Synthetic seismograms calculated from a velocity model with a layer of underplate at 31.5 km depth. (d) Synthetic seismograms calculated from a model with a layer of underplate of a constant thickness of 4 km.

Figure 14: (a) Vertical geophone section of OBS 35. (b) Synthetic seismograms calculated from the final velocity model (velocity depth function at the OBS is shown in inset). (c) Synthetic seismograms calculated from a velocity model with oceanic type velocity gradients (velocity depth function at the OBS is shown in inset).

Figure 15: Relationship between velocity and density from various publications. Coloured crosses mark velocity and corresponding densities used for gravity modelling of both profiles. Grey shaded areas mark the error bounds of 0.05 kg/m^3.

Figure 16: Free air gravity anomaly in the NE Rockall Trough from satellite altimetry *Sandwell and Smith* [1995], contoured every 25 mGal. The gravity anomaly south over Rosemary Bank south of Line E causes a discrepancy between measured gravity by satellite and predicted gravity anomaly from modelling.

Figure 17: Fit between the predicted gravity anomaly (broken line) and the measured free air anomaly from satellite altimetry (solid line) on Line E. Crustal P-wave velocities

from the seismic models were converted to densities using the relationship of Christensen and Mooney (1995) and others (Figure 15) with upper mantle densities set to a constant 3.32 g/cm^3. Unconstrained parts of the velocity model have been changed to improve the fit of the gravity.

Figure 18: Fit between the predicted gravity anomaly (broken line) and the measured free air anomaly from satellite altimetry (solid line) on Line D. Crustal P-wave velocities from the seismic models were converted to densities using the relationship of Christensen and Mooney (1995) and others (Figure 15) with upper mantle densities set to a constant 3.32 g/cm^3.

Figure 19: (a) Solid lines: digitised reflectors from reflection seismic section of the BANS profile. Broken lines: boundaries from the velocity model converted to TWT (b) Final velocity model including the model boundaries used during inversion (solid lines) and isovelocity contours every 0.25 km/s. Positions of sonobuoys (circles) and ESPs (inverted triangles) are indicated. (c) Ray coverage of the model of Line E for the sedimentary layers, with every 20^{th} ray from point-to-point raytracing. Vertical bars indicate the cross points with the perpendicular ESPs. Density values used in the gravity modelling are annontated (d) Fit between the travel time picks (dark grey bars) and the predicted arrival times (black lines) from raytracing for the sedimentary layers (e) Fit between the predicted gravity anomaly (broken line) and the measured free air anomaly from satellite altimetry (solid line). Density values used in the gravity modelling are annontated in (c)

Figure 20: Data from BANS EPS 06 at ocean-continent boundary, showing a double reflection characteristic of an igneous underplate body.

Figure 21: Geological cross sections based on the velocity models of (a) Line E (b) Bans (c) Line D.

Figure 22: Comparison of velocity-depth profiles for the PUMA experiment (dashed lines) *Powell and Sinha* [1987] and Line E (solid line) at 480 km model distance.

Figure 23: Comparison of velocity-depth profiles for the Line P88-2 *Roberts et al.* [1988] and Line E. (a) Comparison of the velocity depth profile of the Line P88-2 (dashed line) and Line E at 80 km model distance (solid line) at Lousy Bank. (b) Comparison of the velocity depth profile of the Line P88-2 (dashed line) and Line E (solid line) at 330 km model distance in the centre of the Rockall Trough. (c) Comparison of the velocity depth profile of the Line P88-2 (dashed line) and Line E (solid line) at 480 km model distance at the continental shelf.

Figure 24: Simplified lithology of well BP 154/3-1 and comparison with the wide-angle velocity model.

Phase	No of picks	RMS traveltime residual	chi-squared
Water	1819	0.041	1.035
Sediments 1 reflection	1632	0.106	3.147
Sediments 2 reflection	826	0.078	1.687
Sediments 3	335	0.167	4.378
Basalt	1134	0.074	1.538
Upper crust	5731	0.095	5.599
lower crust	1373	0.081	1.828
Mid-crustal reflection (oc.)	305	0.206	4.263
PmP/Top underplate	2219	0.199	3.962
Base underplate	691	0.128	2.562
Pn	149	0.264	10.995
All Phases	16214	0.118	3.681

Table 1. Traveltime residuals and chi-squared error for all phases and the complete model of Line E.

Phase	No of picks	RMS traveltime residual	chi-squared
Water	2292	0.037	1.045
Sediments 1	1016	0.059	0.728
Sediments 2	403	0.050	0.709
Sediments 3	1751	0.110	2.441
Basalt	2520	0.073	1.630
Upper crust	2252	0.140	11.727
Mid-crustal reflection (oc.)	133	0.034	0.477
PmP/Top underplate	1066	0.251	8.860
Base underplate	131	0.069	1.937
Pn	427	0.147	3.372
All Phases	11991	0.110	3.662

Table 2. Traveltime residuals and chi-squared error for all phases and the complete model of Line D.

	Phase	No of picks	RMS traveltime residual	chi-squared
BANS 1	Water	154	0.134	2.805
	Water Refl.	534	0.074	0.853
	Basalt	583	0.065	0.670
	Crust	952	0.081	1.025
	PmP	102	0.053	0.448
	All Phases	2325	0.079	0.987
BANS ESP 02	All Phases	695	0.093	1.364
BANS ESP 06	All Phases	888	0.124	2.403
V 89-6	All Phases	419	0.071	0.780

Table 3. Traveltime residuals and chi-squared error for all phases and the complete models.

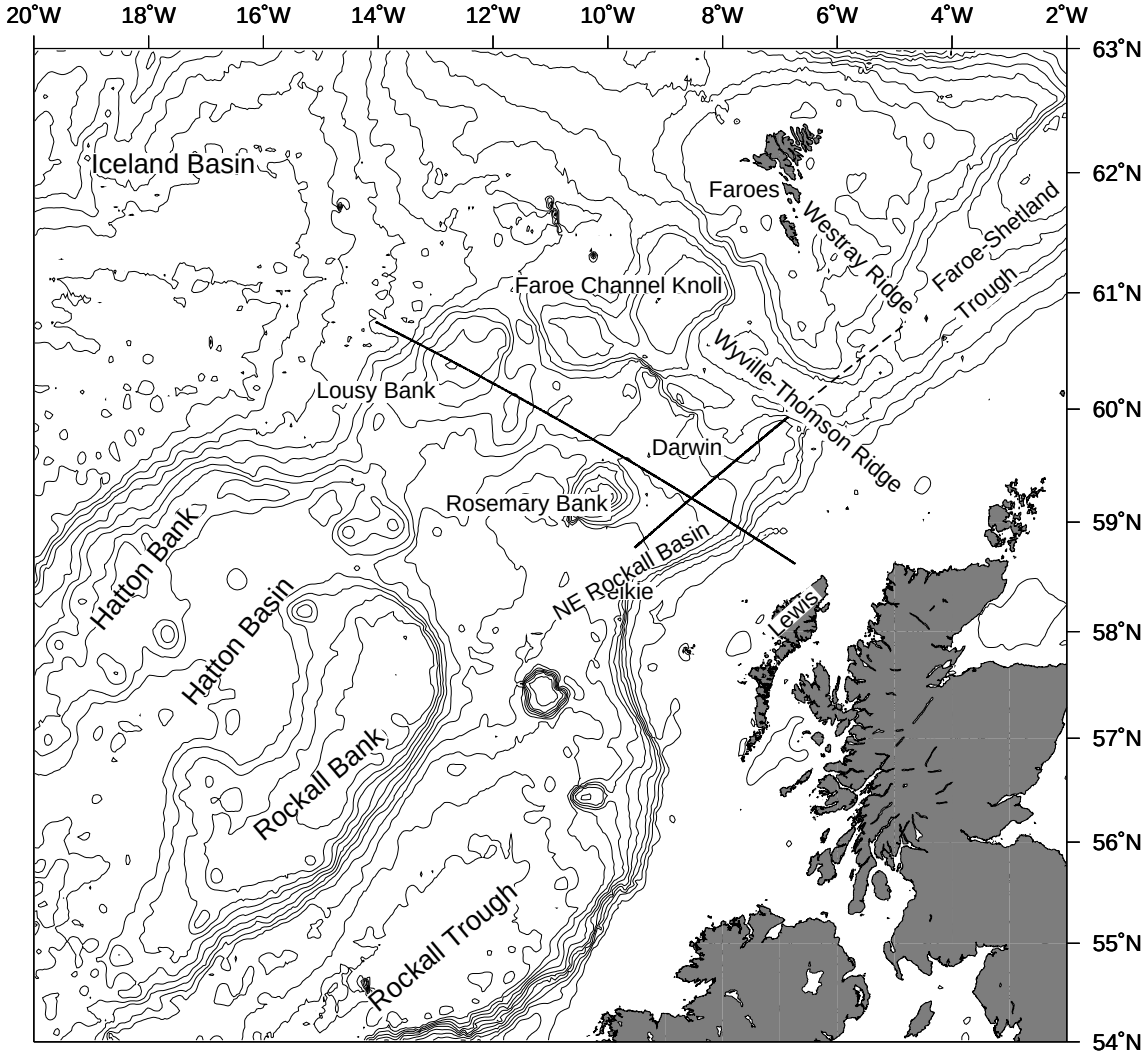
20°W
18°W
16°W
14°W
12°W
10°W
8°W
6°W
4°W
2°W
63°N
62°N
61°N
60°N
59°N
58°N
57°N
56°N
55°N
54°N
Iceland Basin
Faroes
Westray Ridge
Faroe-Shetland
Trough
Faroe Channel Knoll
Wyville-Thomson Ridge
Lousy Bank
Darwin
Rosemary Bank
NE Rockall Basin
Hatton Bank
Hatton Basin
Rockall Bank
Rockall Trough
Lewis

Figure 1.

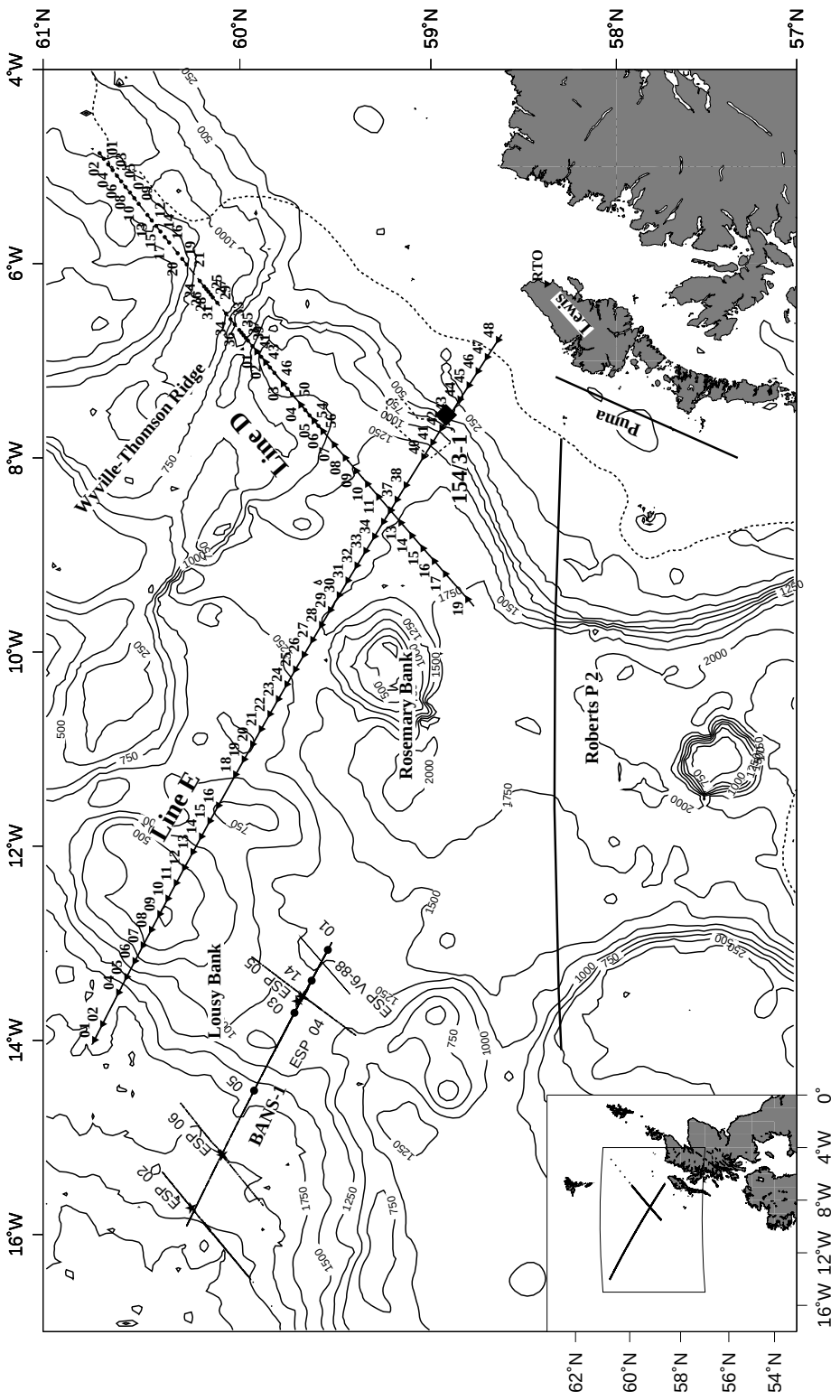
Wyville-Thomson Ridge
Line D
154/3-1
Puma
Rosemary Bank
Roberts P 2
Line E
Lousy Bank
ESP 01
ESP 02
ESP 03
ESP 04
ESP 05
ESP 06
ESP V6-88
BANS-1
61°N
60°N
59°N
58°N
57°N
4°W
6°W
8°W
10°W
12°W
14°W
16°W
62°N
60°N
58°N
56°N
54°N
16°W 12°W 8°W 4°W 0°

Figure 2.

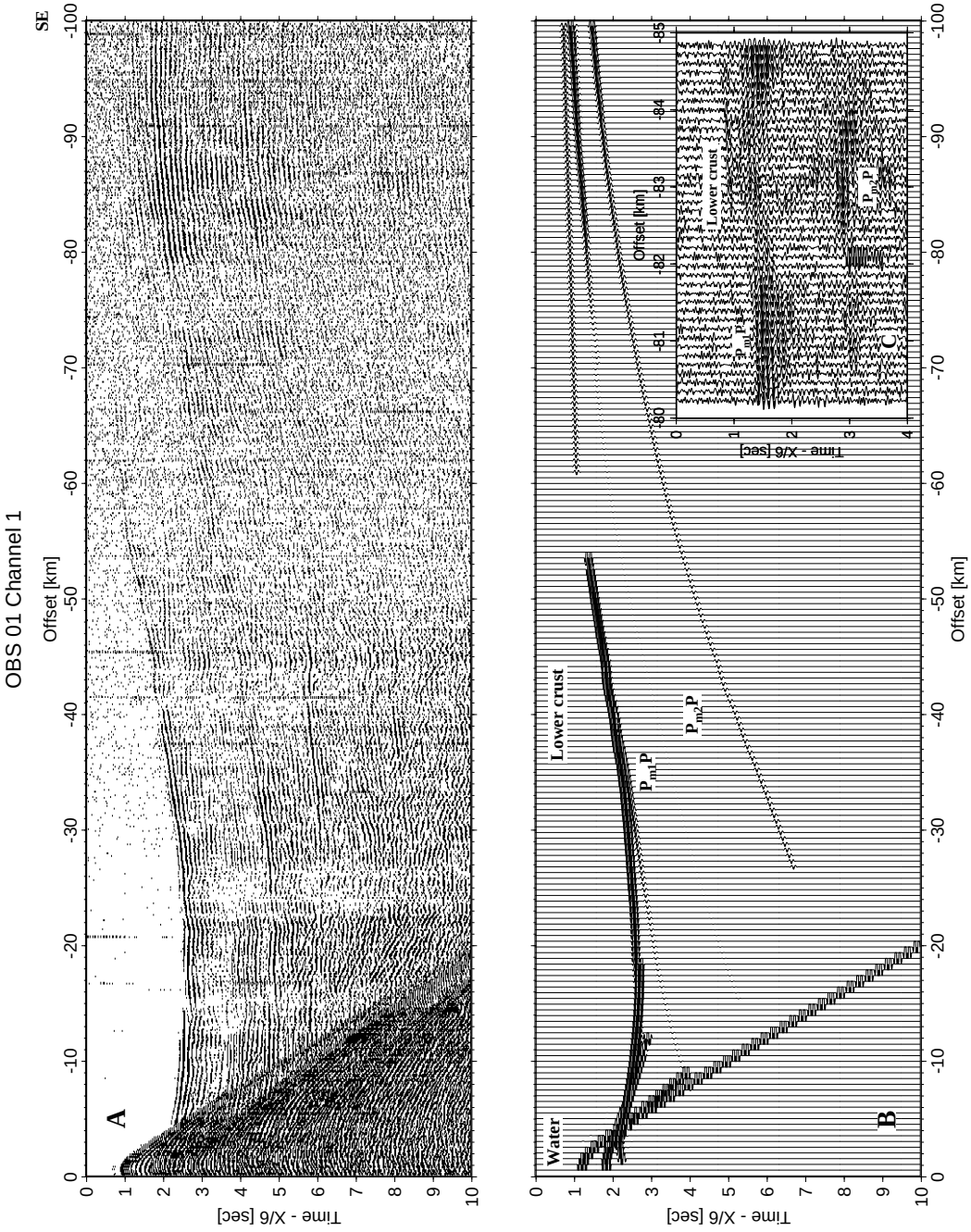
OBS 01 Channel 1
SE
Offset [km]
Time - X/6 [sec]
A
B
C
Water
Lower crust
$P_{m1}P$
$P_{m2}P$
$P_{m1}P_{L1}P$
$P_{m2}P_{L2}P$
$P_{L1}P_{L2}P$

Figure 3.

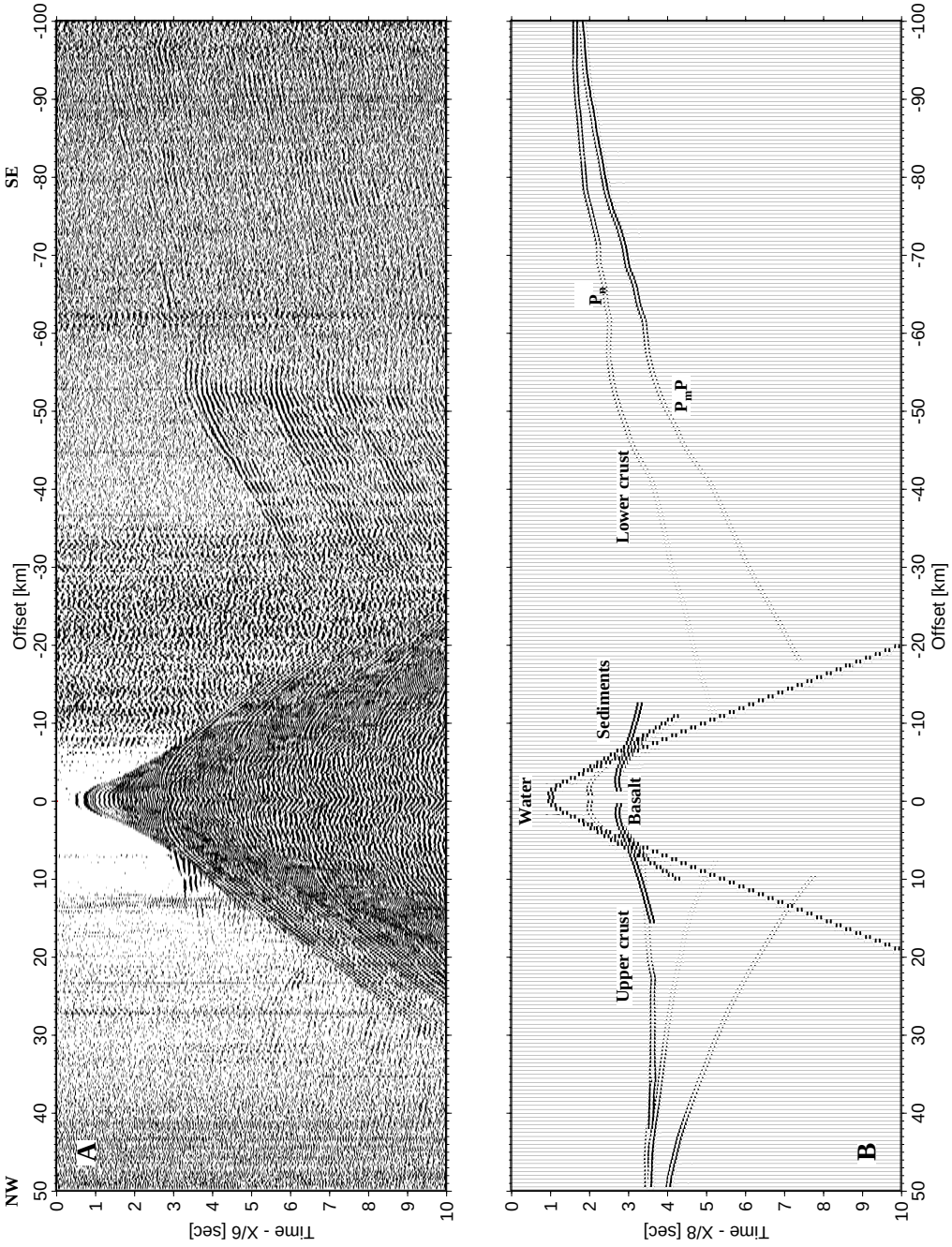
NW
SE
Offset [km]
Time - X/6 [sec]
A
Water
Sediments
Basalt
Upper crust
Lower crust
P_g
P_mP
B
Time - X/8 [sec]

Figure 4.

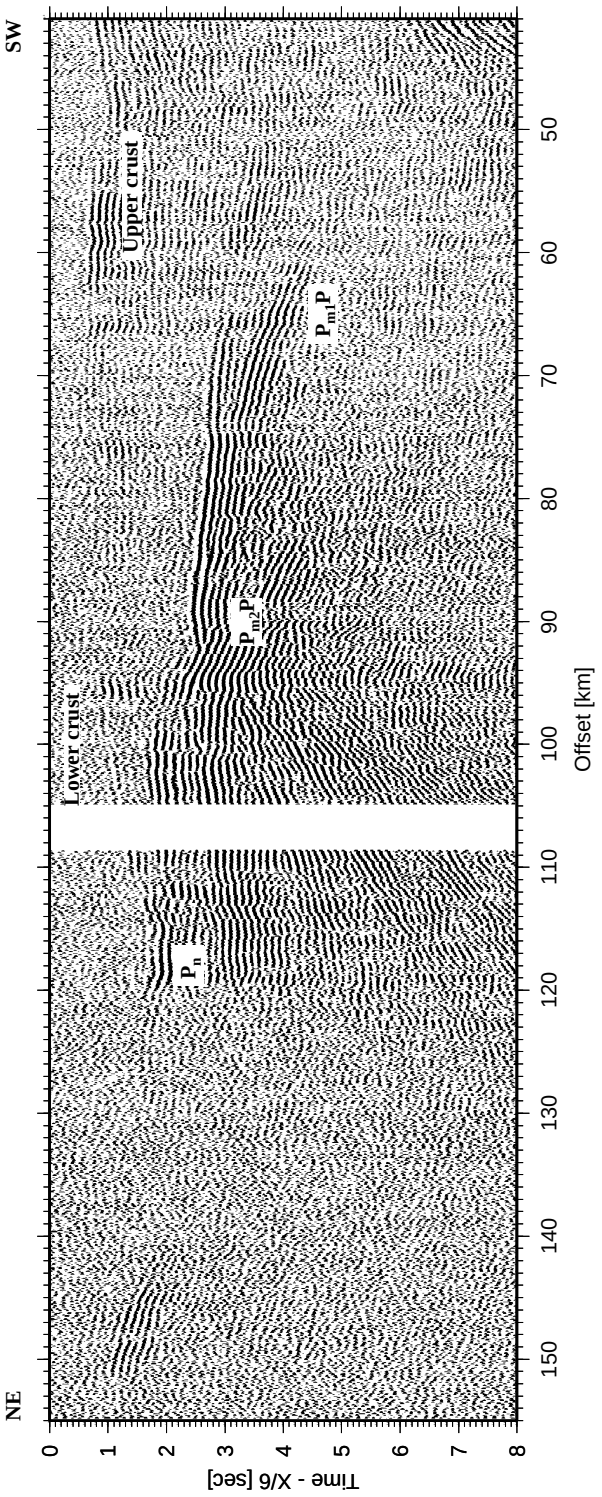
SW
NE
Upper crust
Lower crust
P_n
$P_{m2}P$
$P_{m1}P$
Offset [km]
Time - X/6 [sec]

Figure 5.

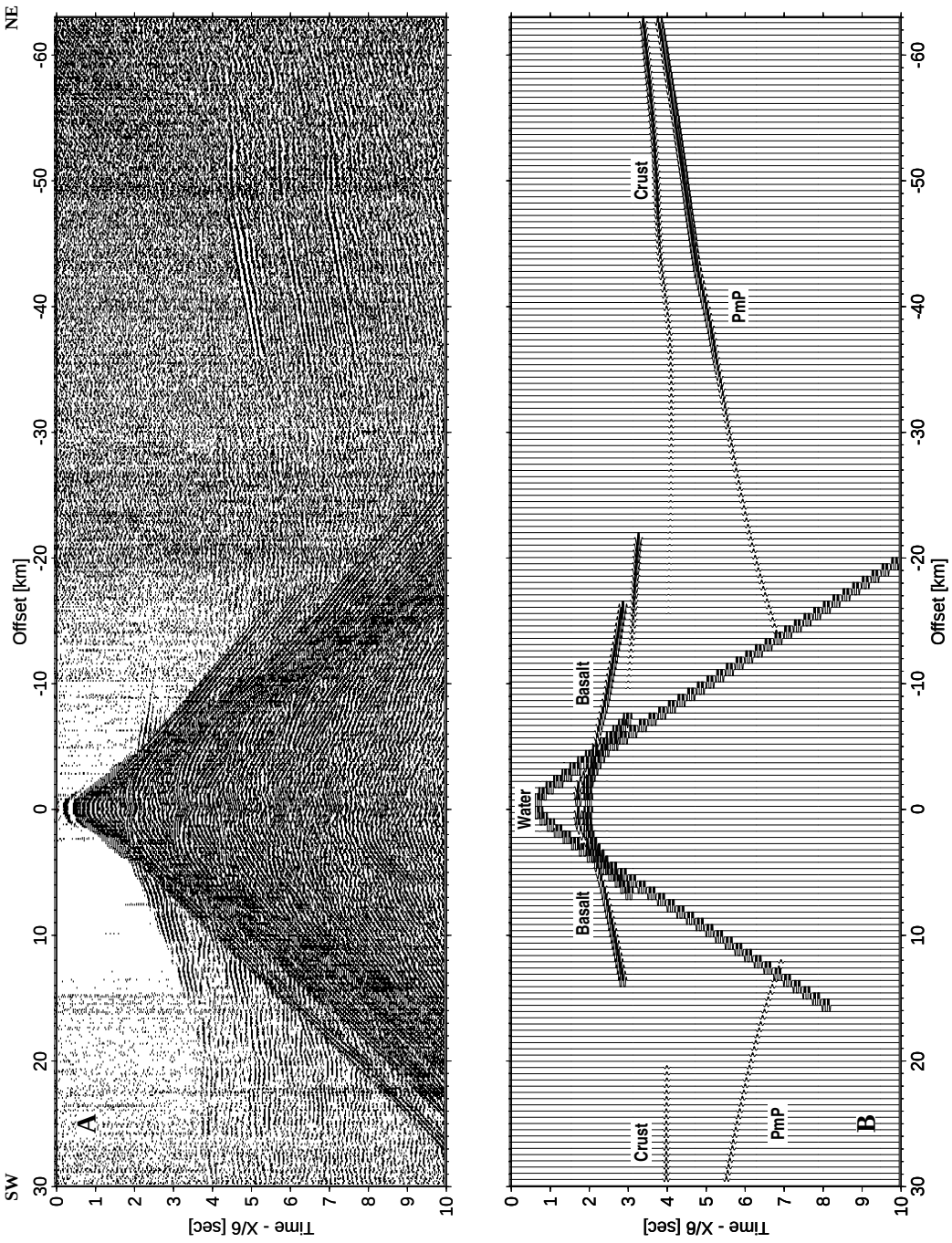
NE
SW
Offset [km]
Time - X/6 [sec]
A
Water
Basalt
Basalt
Crust
PmP
Crust
PmP
B

Figure 6.

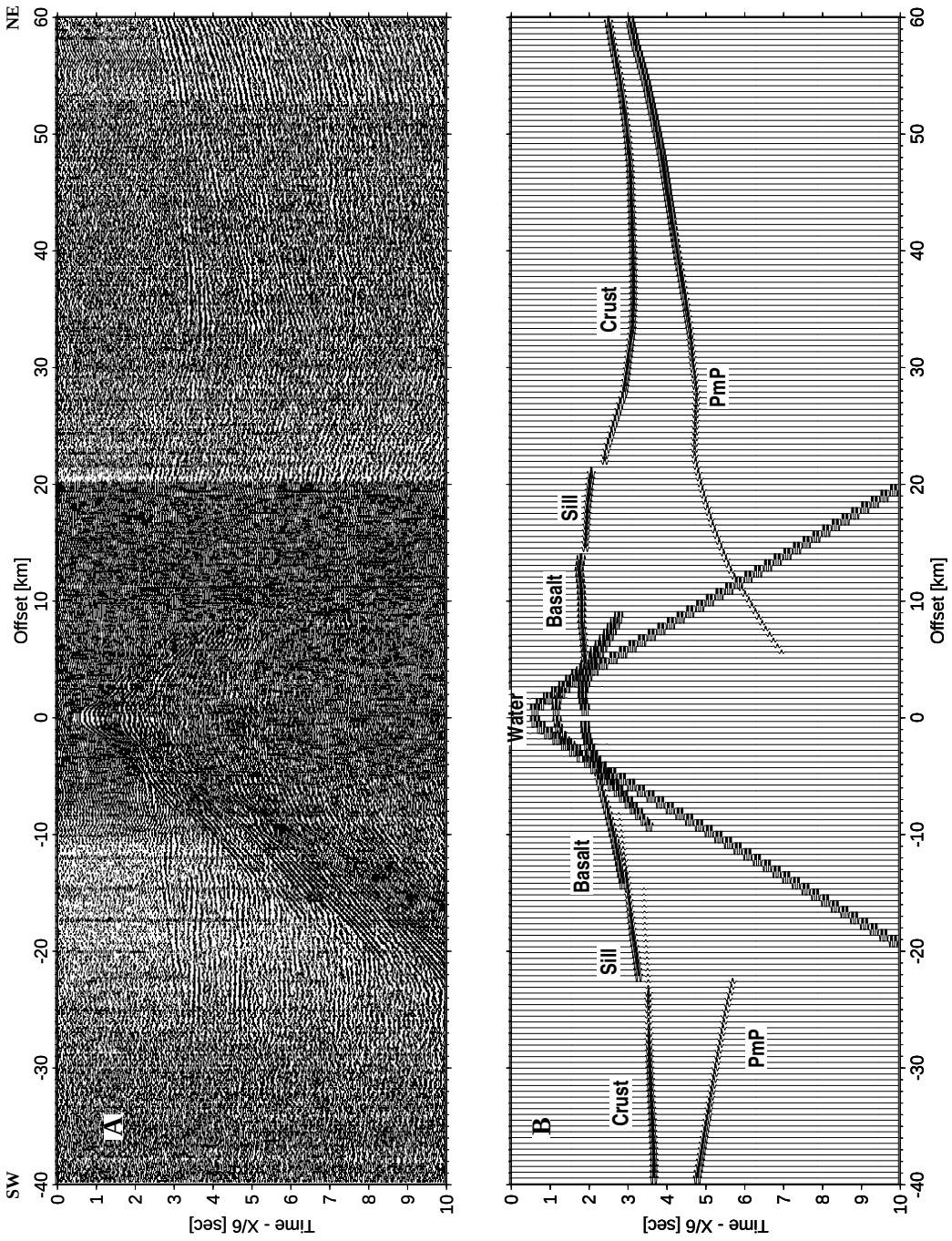
NE
SW
Offset [km]
Time - X/6 [sec]
A
B
Water
Basalt
Sill
Crust
PmP
Basalt
Sill
Crust
PmP

Figure 7.

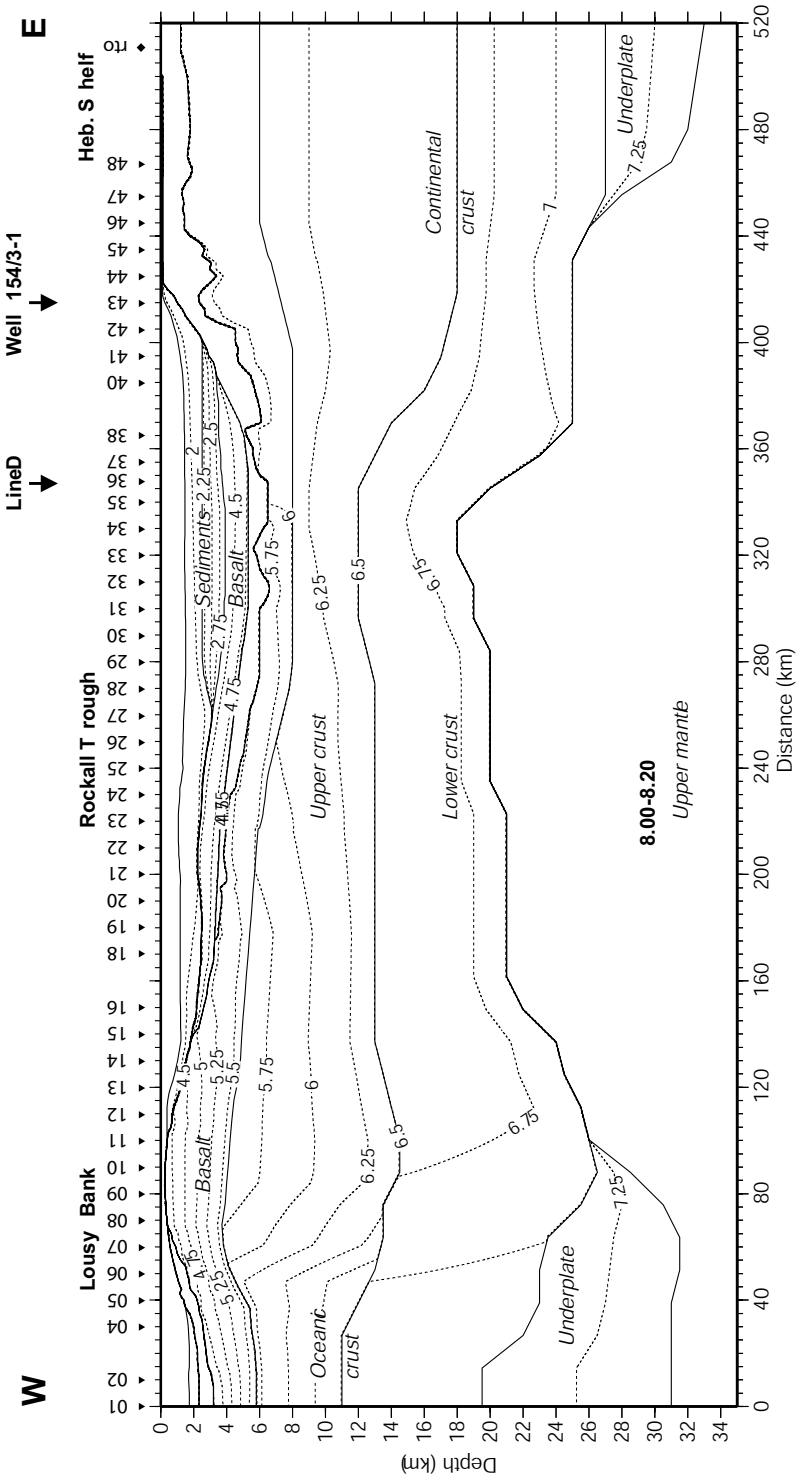
W
E
Lousy Bank
Rockall T rough
Heb. S helf
LineD
Well 154/3-1
Sediments
Basalt
Upper crust
Lower crust
Oceanic crust
Continental crust
Underplate
Upper mantle
8.00-8.20
Depth (km)
Distance (km)

Figure 8.

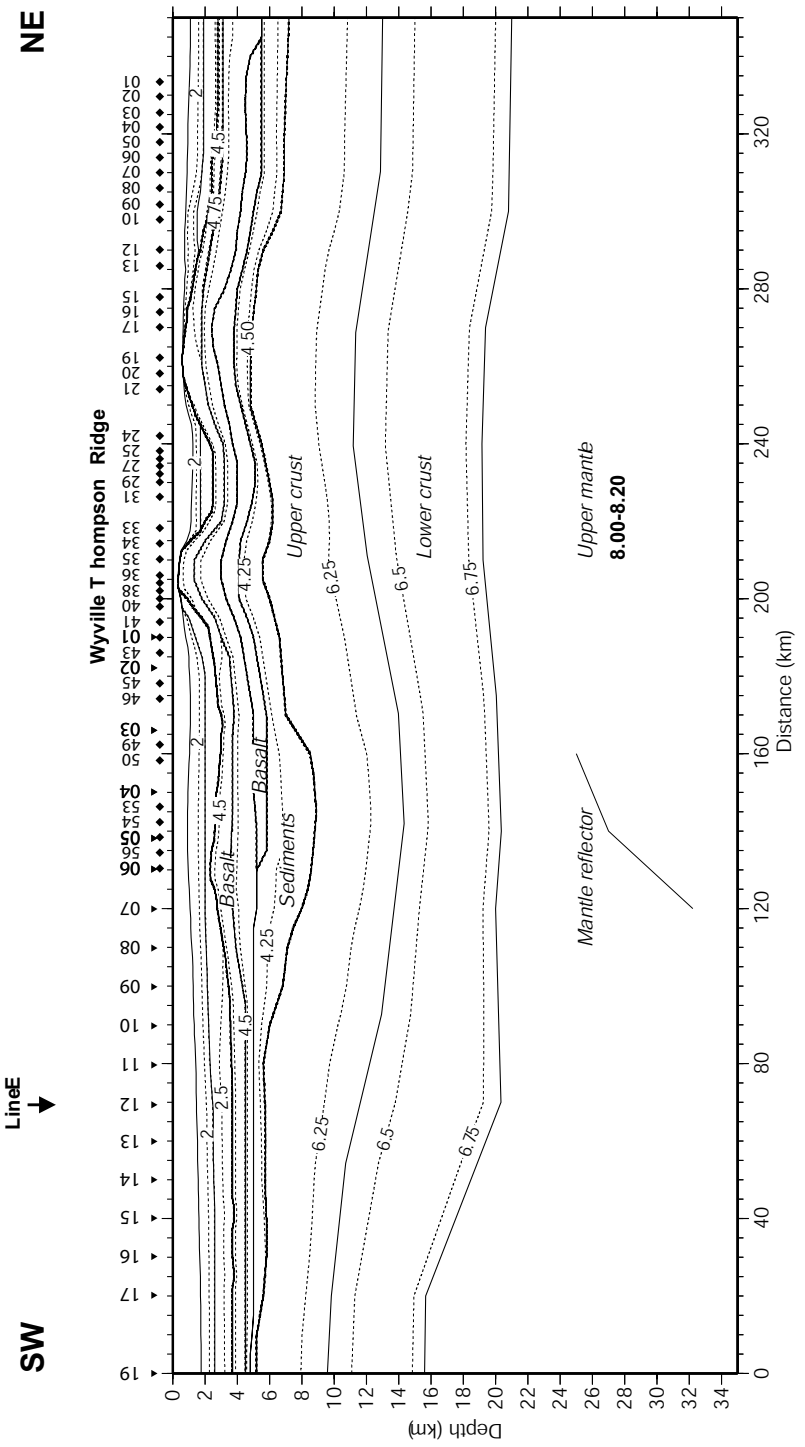
NE
SW
Line E
Wyville T hompson Ridge
Upper crust
Lower crust
Upper mantle
8.00-8.20
Basalt
Basalt
Sediments
Mantle reflector
2
2.5
4.5
4.25
4.50
4.75
6.25
6.5
6.75
Depth (km)
Distance (km)

Figure 9.

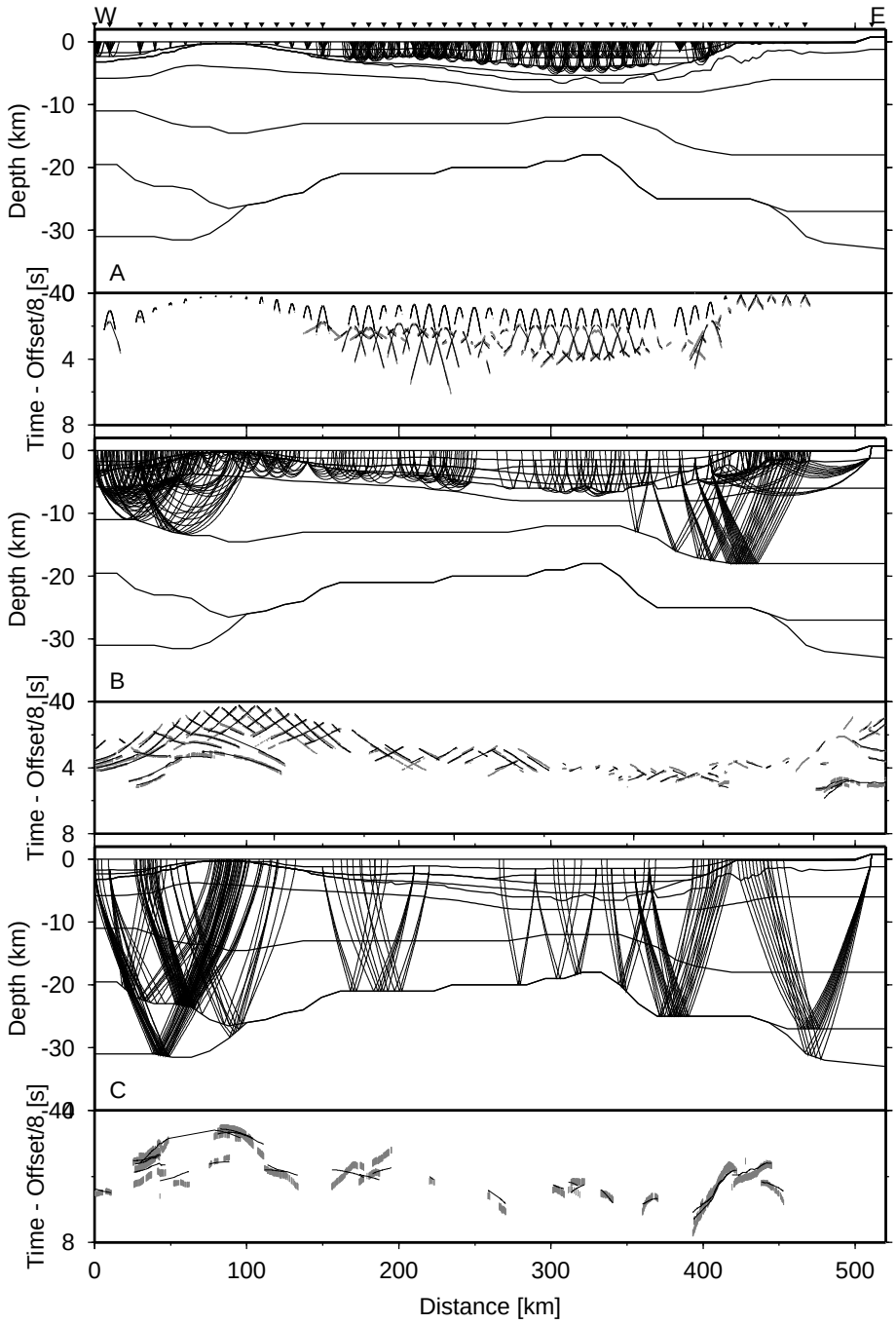
W
E
Depth (km)
0
-10
-20
-30
A
Time - Offset/8 [s]
0
4
8
B
C
0
100
200
300
400
500
Distance [km]

Figure 10.

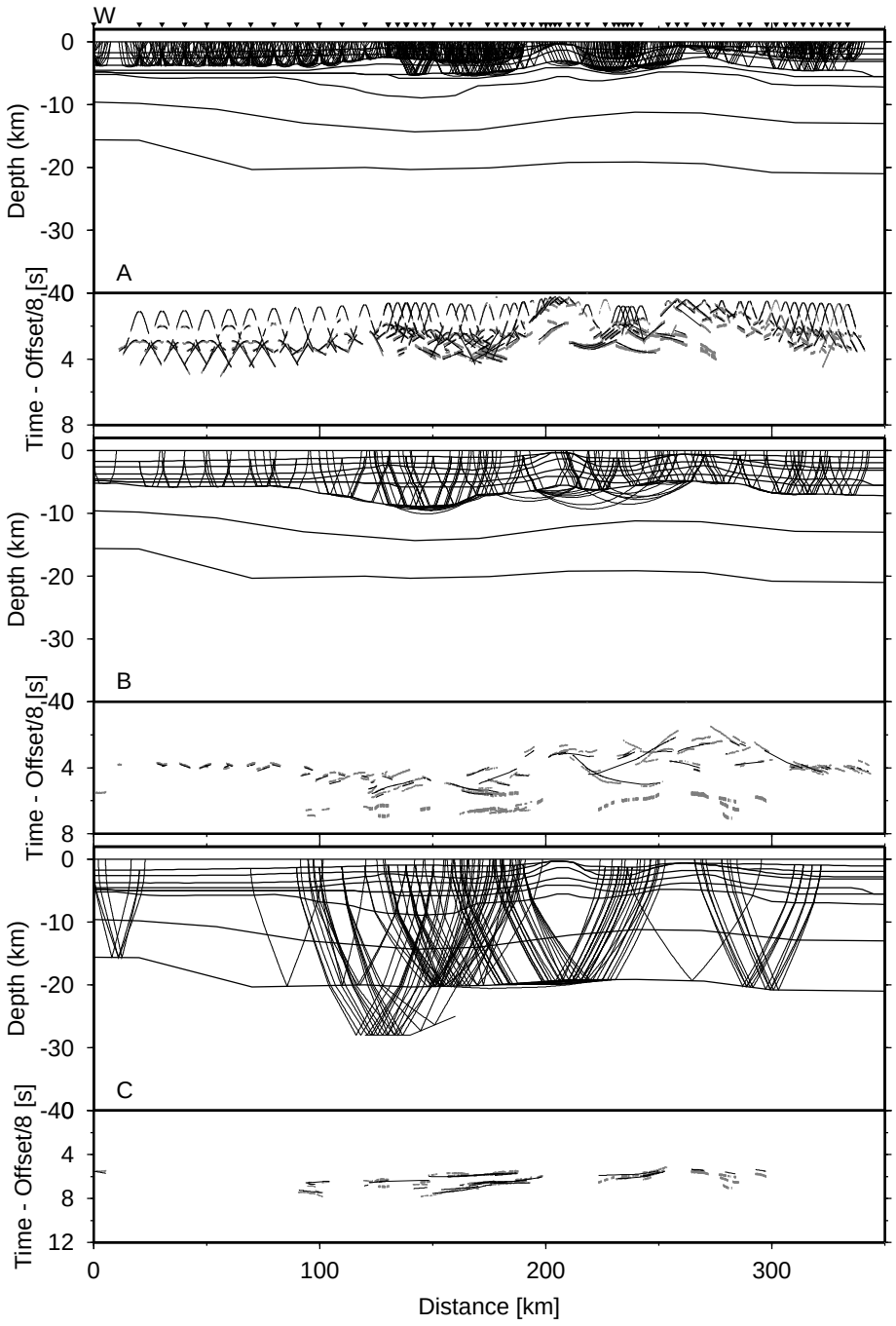

Figure 11.

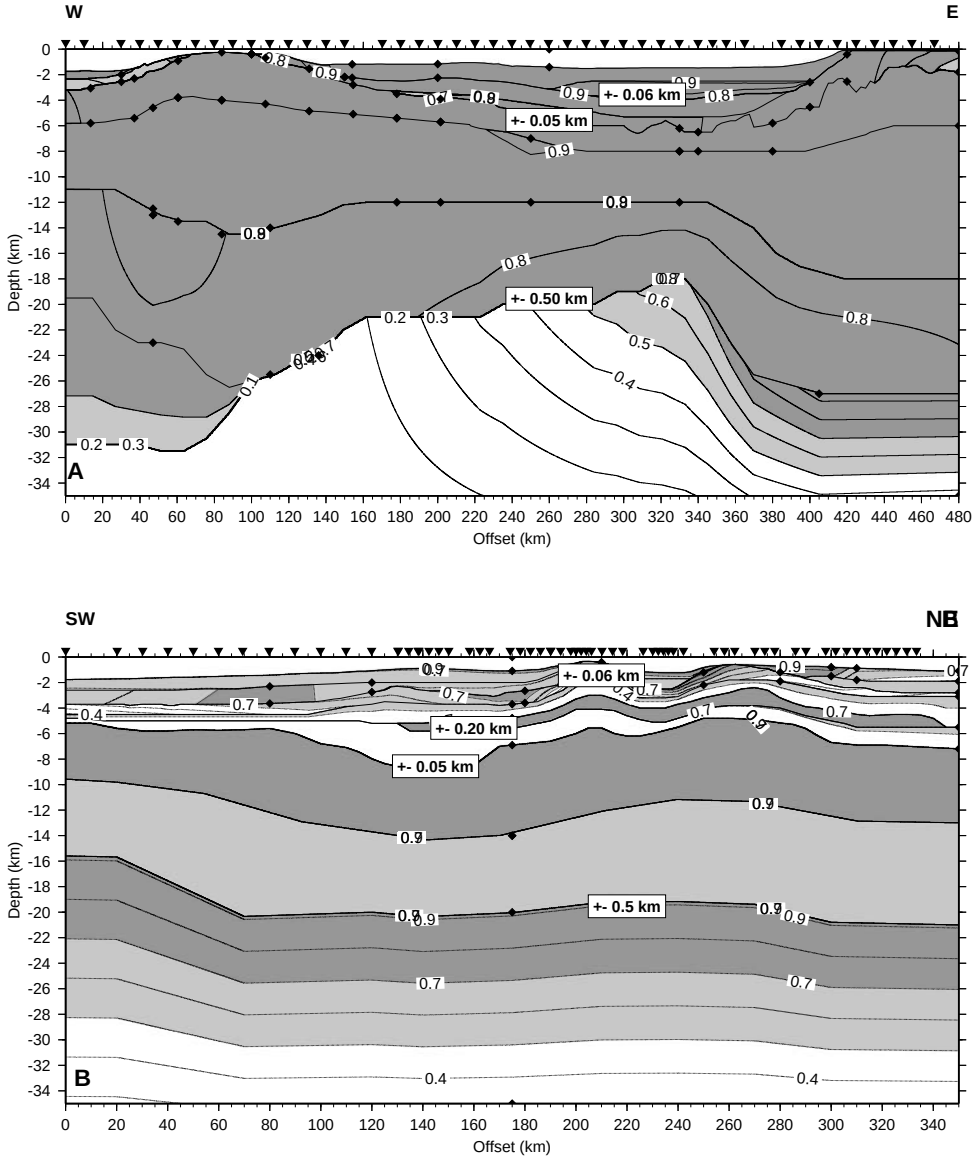
W
E
+- 0.06 km
+- 0.05 km
+- 0.50 km
Depth (km)
Offset (km)
A
SW
NE
+- 0.06 km
+- 0.20 km
+- 0.05 km
+- 0.5 km
Depth (km)
Offset (km)
B

Figure 12.

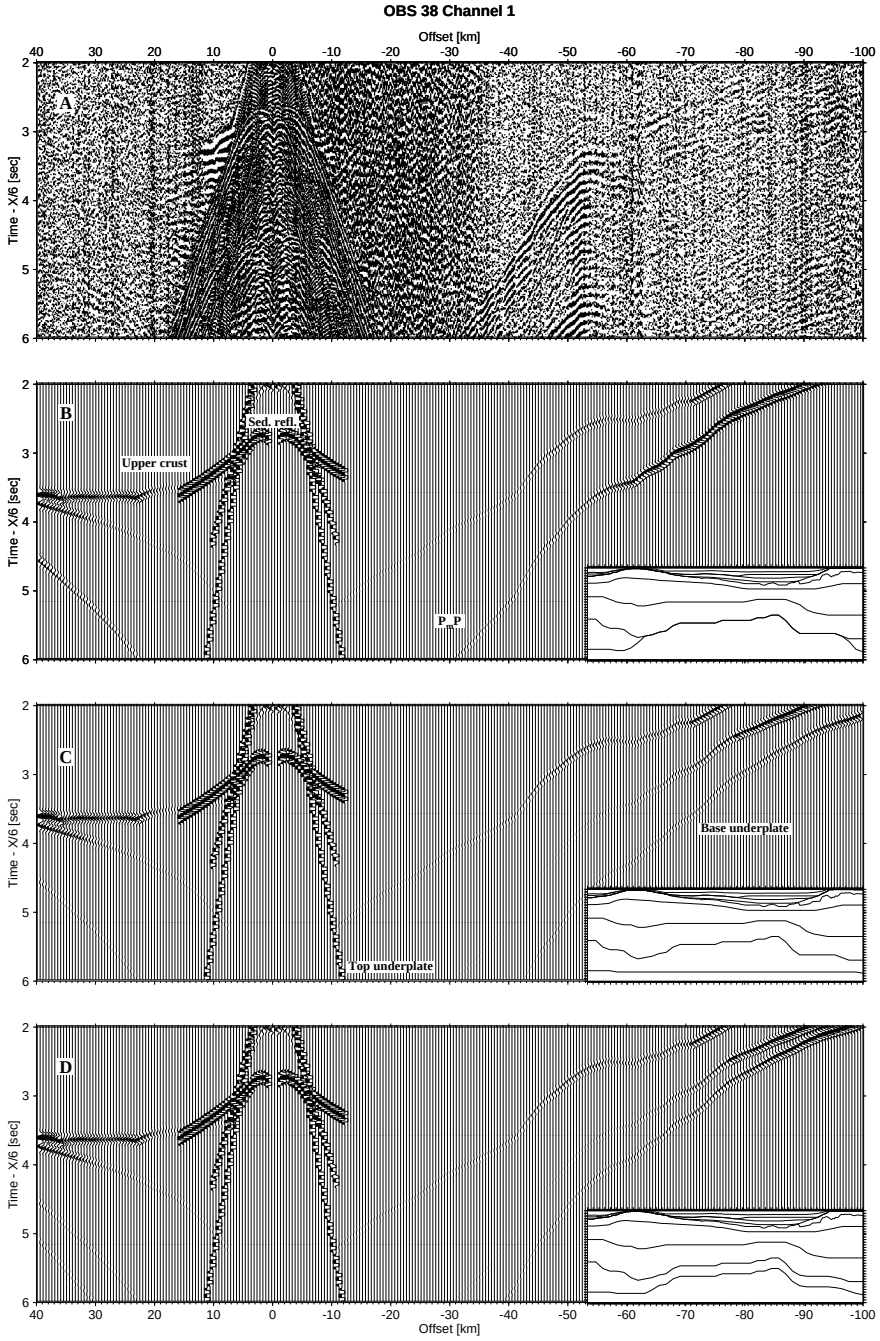
OBS 38 Channel 1
Offset [km]
Time - X/6 [sec]
A
B
Sed. refl.
Upper crust
P_n P
C
Base underplate
Top underplate
D

Figure 13.

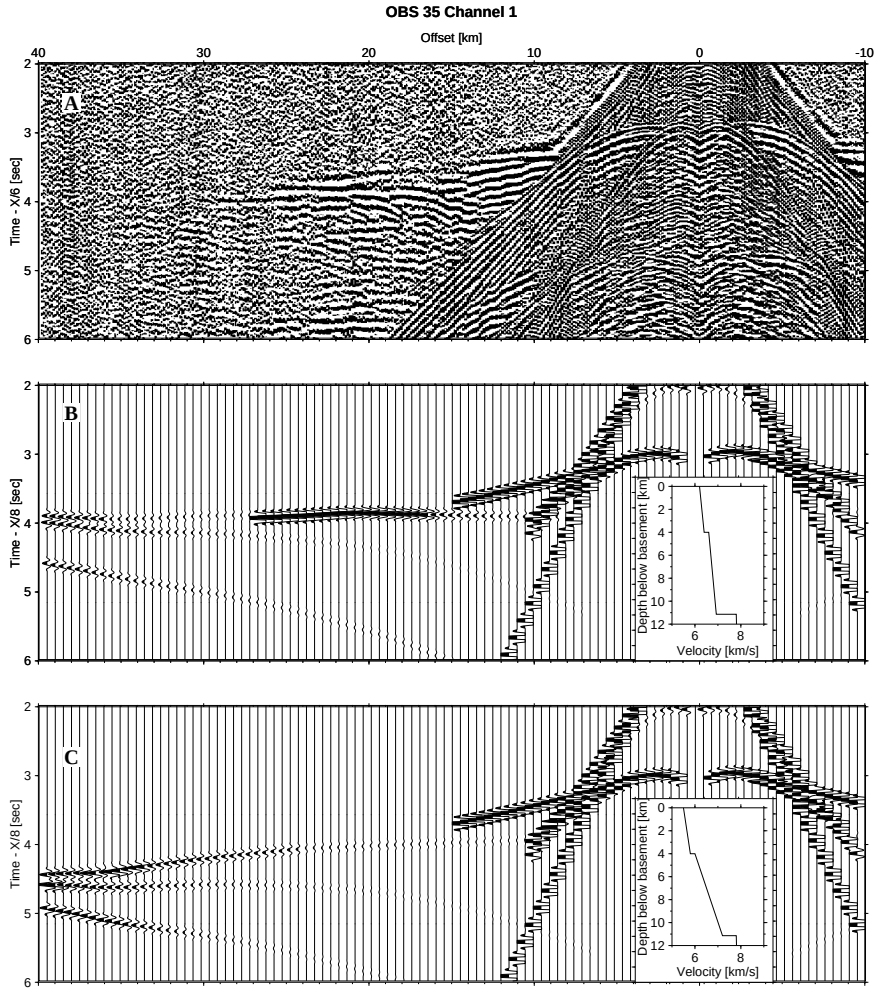
OBS 35 Channel 1
Offset [km]
40
30
20
10
0
-10
A
B
C
Time - X/6 [sec]
Time - X/8 [sec]
Depth below basement [km]
Velocity [km/s]

Figure 14.

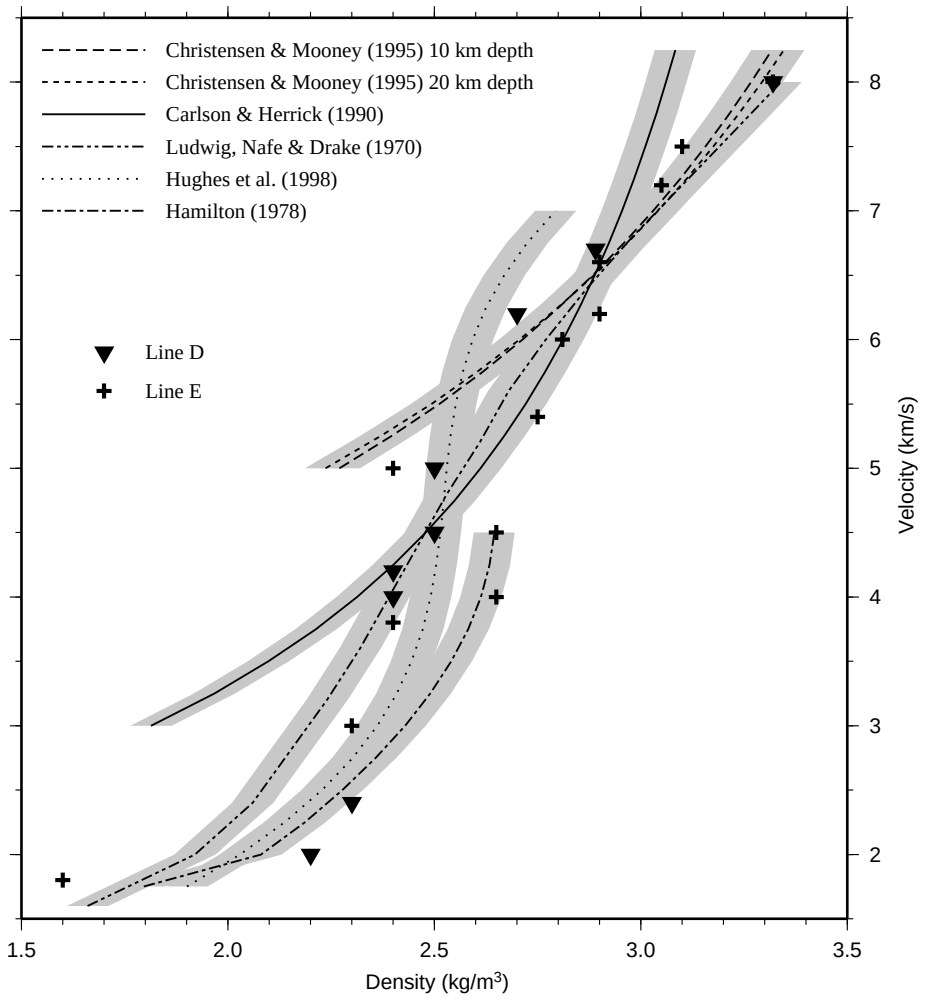
Christensen & Mooney (1995) 10 km depth
Christensen & Mooney (1995) 20 km depth
Carlson & Herrick (1990)
Ludwig, Nafe & Drake (1970)
Hughes et al. (1998)
Hamilton (1978)
Line D
Line E
Velocity (km/s)
Density (kg/m3)
1.5
2.0
2.5
3.0
3.5
2
3
4
5
6
7
8

Figure 15.

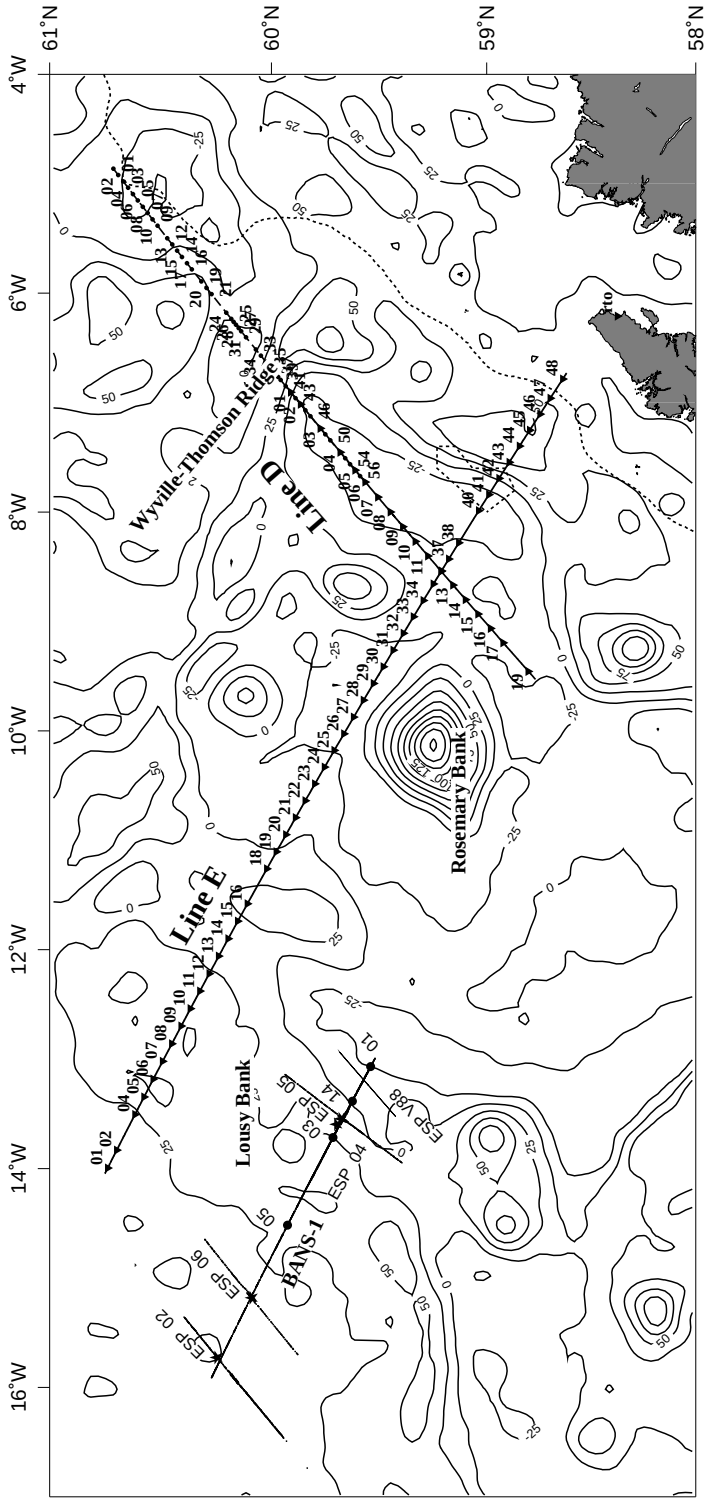
61°N
60°N
59°N
58°N
4°W
6°W
8°W
10°W
12°W
14°W
16°W
Wyville-Thomson Ridge
Line D
Line E
Rosemary Bank
Lousy Bank
BANS-1
ESP 01
ESP 02
ESP 03
ESP 04
ESP 05
ESP 06
ESP V88

Figure 16.

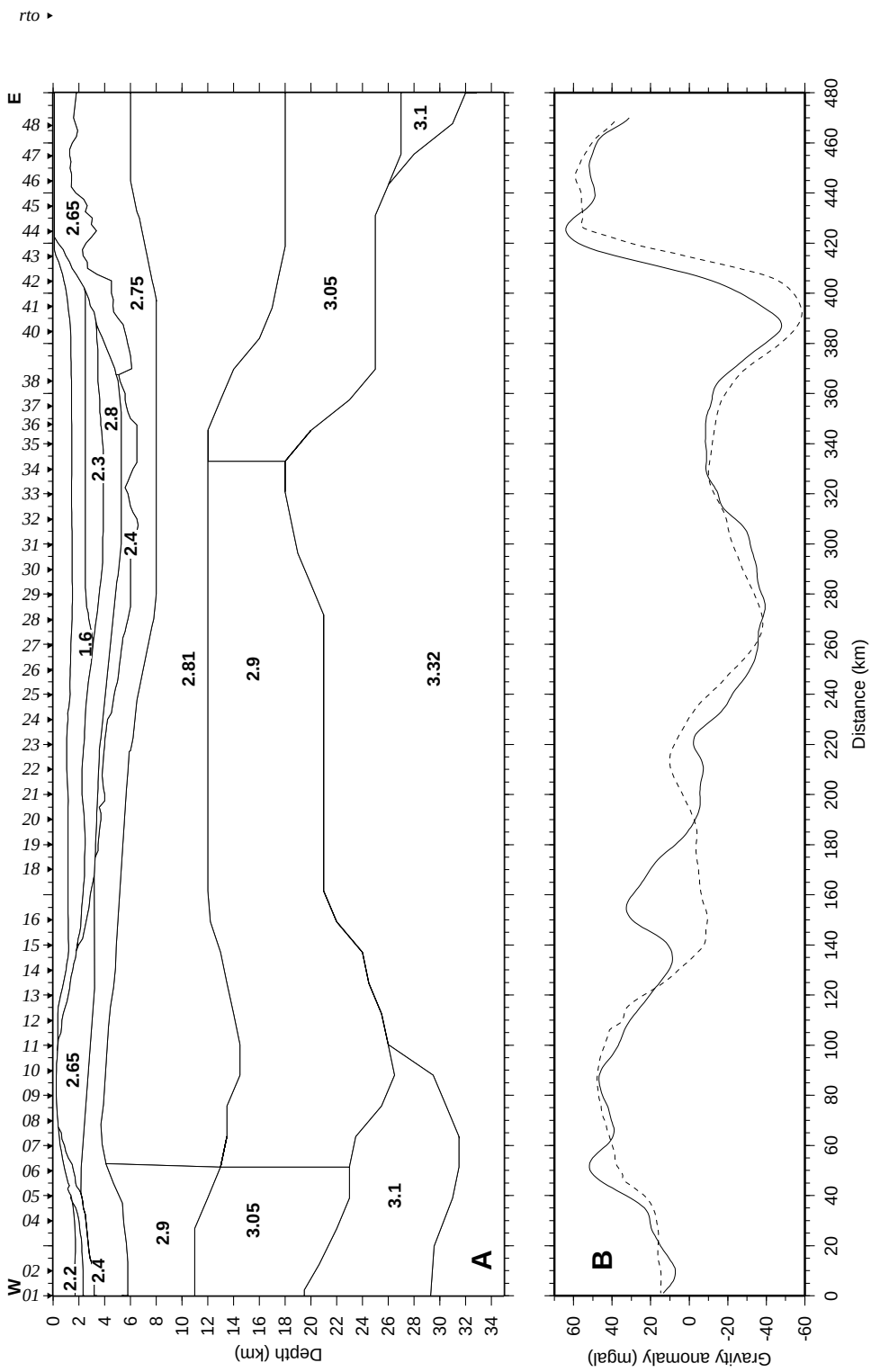
rto
E
W
2.65
2.75
2.8
2.3
2.4
1.6
2.81
2.9
3.32
3.1
3.05
2.2
2.4
2.65
2.9
3.05
3.1
A
B
Depth (km)
Gravity anomaly (mgal)
Distance (km)

Figure 17.

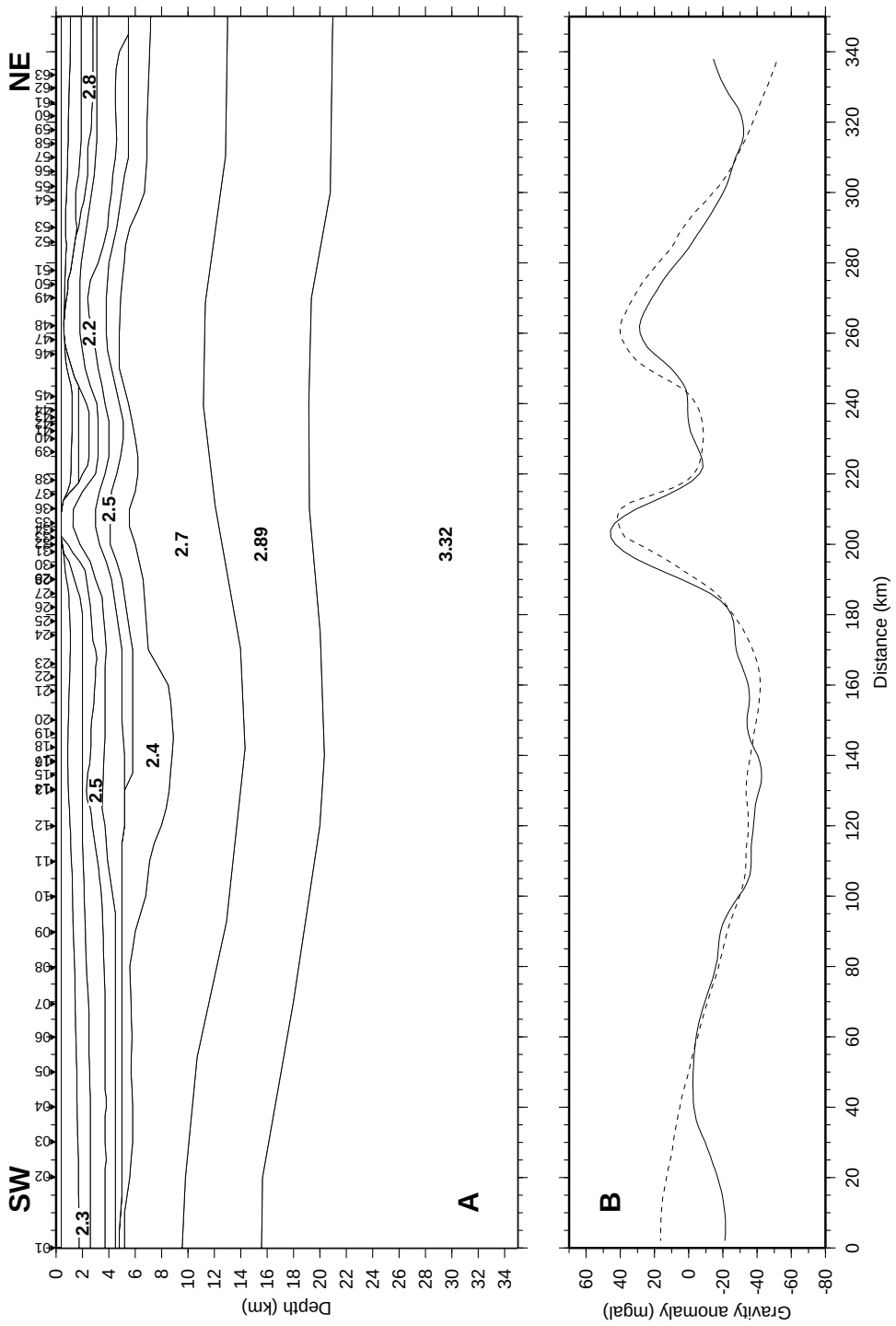
SW
NE
2.3
2.5
2.4
2.5
2.2
2.8
2.5
2.7
2.89
3.32
A
B
Depth (km)
Gravity anomaly (mgal)
Distance (km)

Figure 18.

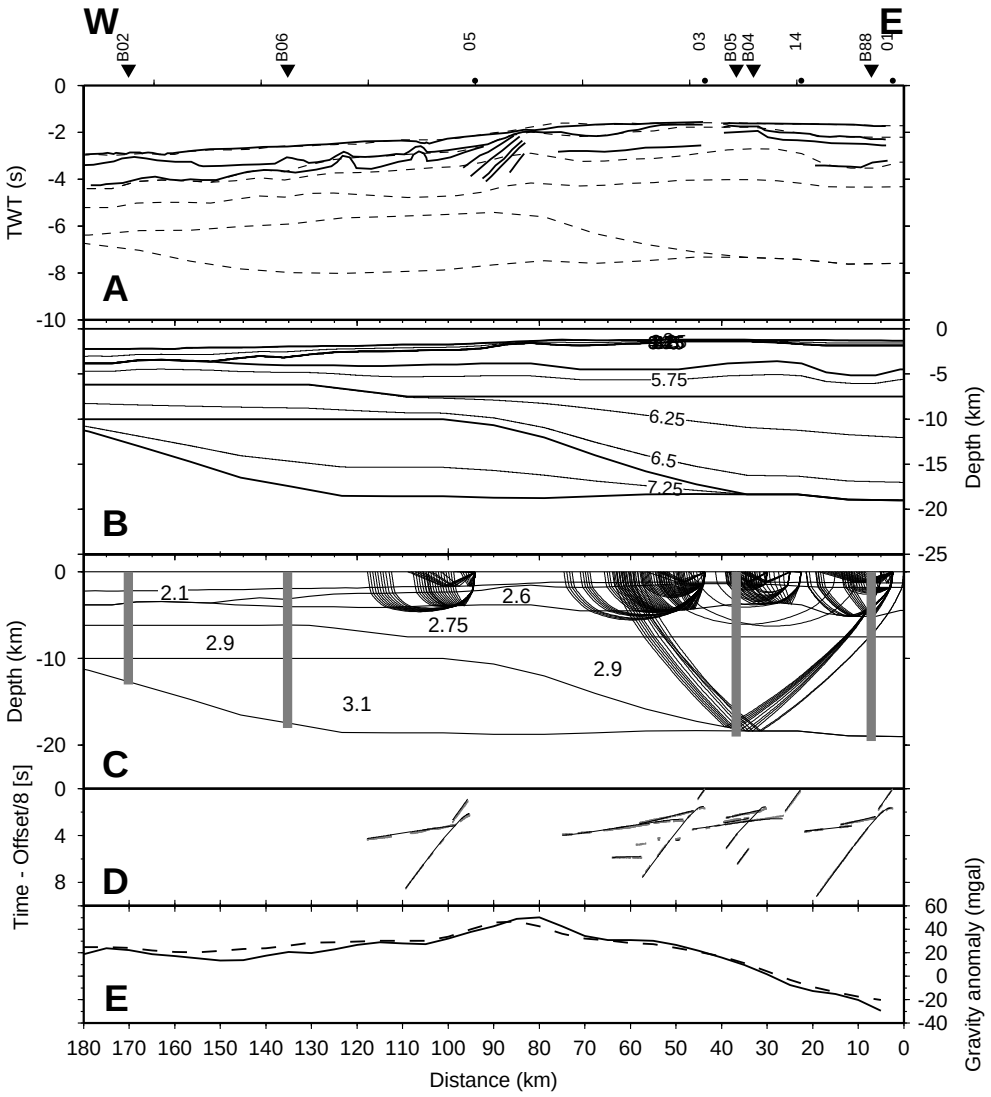
W
E
B02
B06
05
03
B05
B04
14
B88
01
TWT (s)
A
B
5.75
6.25
6.5
7.25
Depth (km)
C
2.1
2.6
2.75
2.9
2.9
3.1
D
Time - Offset/8 [s]
E
Gravity anomaly (mgal)
180 170 160 150 140 130 120 110 100 90 80 70 60 50 40 30 20 10 0
Distance (km)

Figure 19.

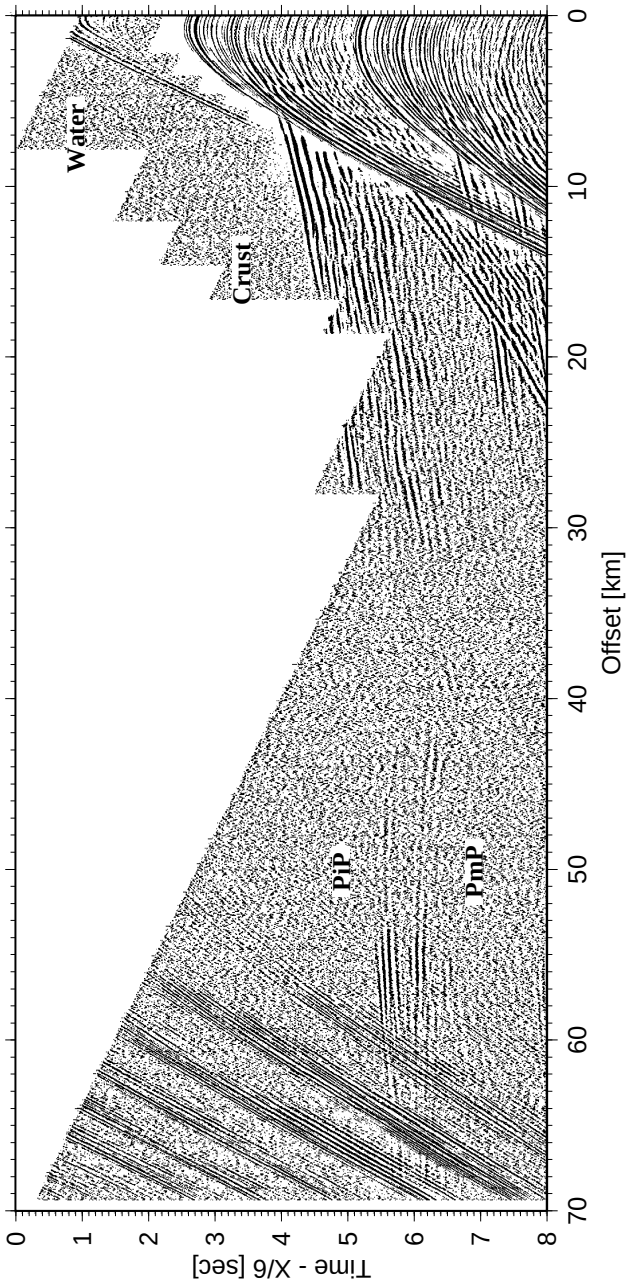
Water
Crust
PiP
PmP
Time - X/6 [sec]
Offset [km]
0
1
2
3
4
5
6
7
8
0
10
20
30
40
50
60
70

Figure 20.

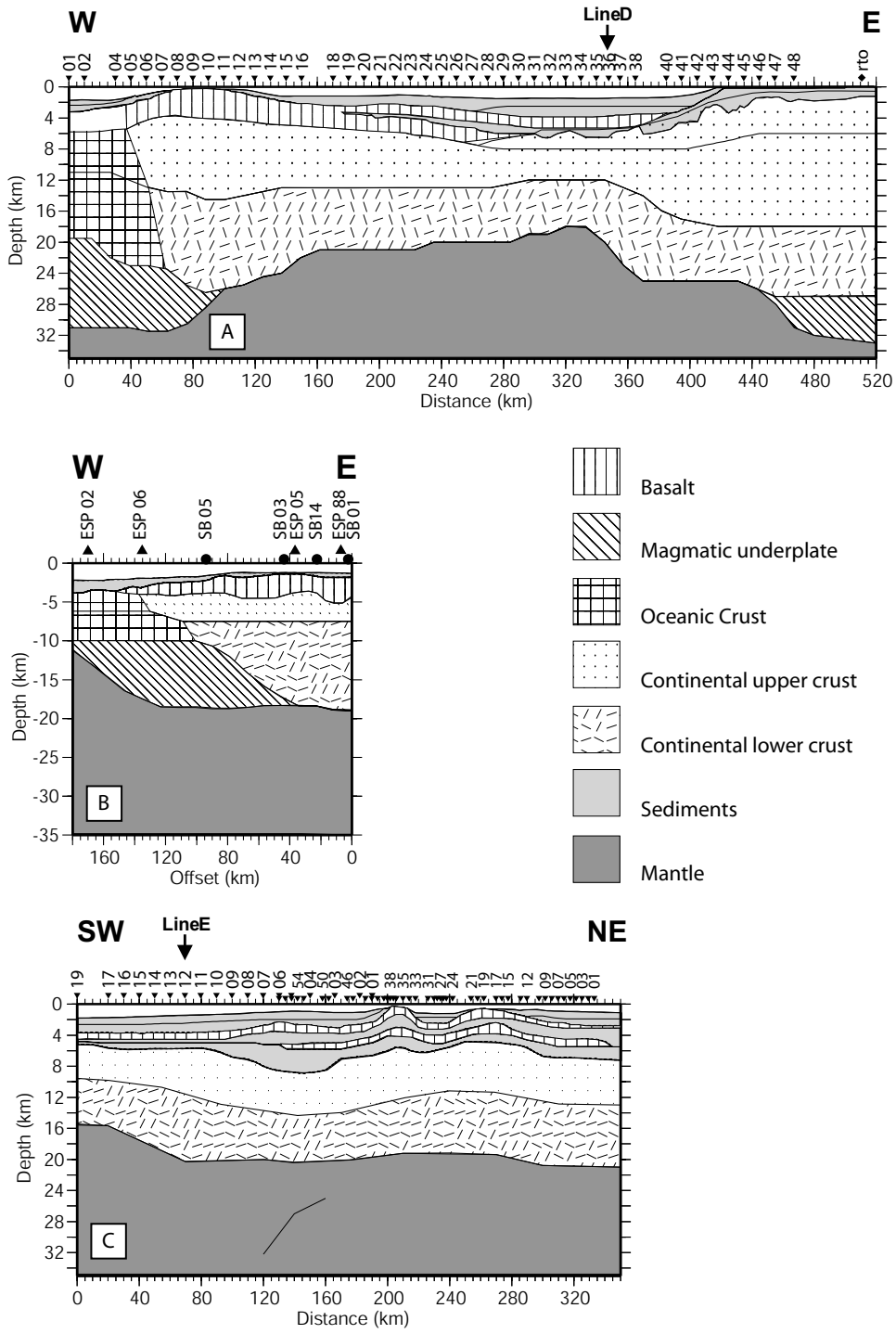
W
LineD
E
Depth (km)
A
Distance (km)
W
E
ESP 02
ESP 06
SB 05
SB 03
ESP 05
SB14
ESP 88
SB 01
Depth (km)
B
Offset (km)
Basalt
Magmatic underplate
Oceanic Crust
Continental upper crust
Continental lower crust
Sediments
Mantle
SW
LineE
NE
Depth (km)
C
Distance (km)

Figure 21.

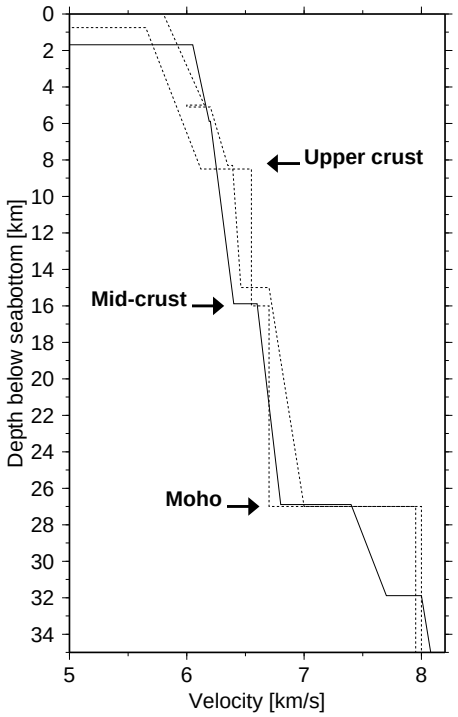

Figure 22.

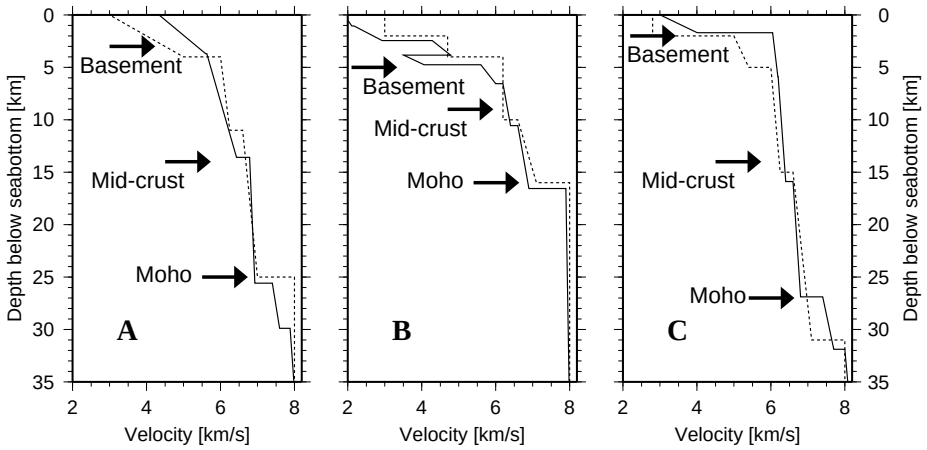

Figure 23.

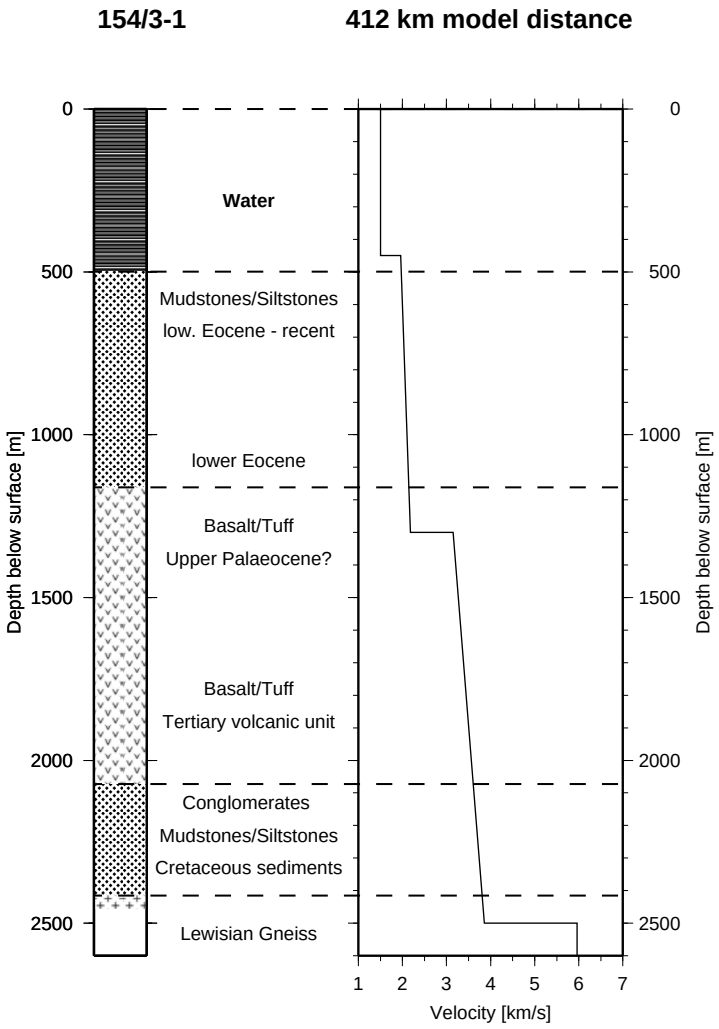
154/3-1
412 km model distance
Water
Mudstones/Siltstones
low. Eocene - recent
lower Eocene
Basalt/Tuff
Upper Palaeocene?
Basalt/Tuff
Tertiary volcanic unit
Conglomerates
Mudstones/Siltstones
Cretaceous sediments
Lewisian Gneiss
Depth below surface [m]
Velocity [km/s]
0
500
1000
1500
2000
2500
1
2
3
4
5
6
7

Figure 24.